# Improved mapping of Jupiter's auroral features to magnetospheric sources

Marissa F. Vogt,[1,2] Margaret G. Kivelson,[1,2,3] Krishan K. Khurana,[1]
Raymond J. Walker,[1,2] Bertrand Bonfond,[1,4] Denis Grodent,[4] and Aikaterini Radioti[4]

Received 29 September 2010; revised 23 December 2010; accepted 7 January 2011; published 18 March 2011.

[1] The magnetospheric mapping of Jupiter's polar auroral emissions is highly uncertain because global Jovian field models are known to be inaccurate beyond ~30 $R_J$. Furthermore, the boundary between open and closed flux in the ionosphere is not well defined because, unlike the Earth, the main auroral oval emissions at Jupiter are likely associated with the breakdown of plasma corotation and not the open/closed flux boundary in the polar cap. We have mapped contours of constant radial distance from the magnetic equator to the ionosphere in order to understand how auroral features relate to magnetospheric sources. Instead of following model field lines, we map equatorial regions to the ionosphere by requiring that the magnetic flux in some specified region at the equator equals the magnetic flux in the area to which it maps in the ionosphere. Equating the fluxes in this way allows us to link a given position in the magnetosphere to a position in the ionosphere. We find that the polar auroral active region maps to field lines beyond the dayside magnetopause that can be interpreted as Jupiter's polar cusp; the swirl region maps to lobe field lines on the night side and can be interpreted as Jupiter's polar cap; the dark region spans both open and closed field lines and must be explained by multiple processes. Additionally, we conclude that the flux through most of the area inside the main oval matches the magnetic flux contained in the magnetotail lobes and is probably open to the solar wind.

**Citation:** Vogt, M. F., M. G. Kivelson, K. K. Khurana, R. J. Walker, B. Bonfond, D. Grodent, and A. Radioti (2011), Improved mapping of Jupiter's auroral features to magnetospheric sources, *J. Geophys. Res.*, *116*, A03220, doi:10.1029/2010JA016148.

## 1. Introduction

[2] Observations of Jupiter's aurora at ultraviolet, infrared, and visible wavelengths show that the emissions can be classified into three main types: the satellite footprints, a main oval (main emissions), and the mysterious polar emissions [*Clarke et al.*, 1998]. These auroral observations, along with interpretive theoretical studies, have helped to constrain global magnetic field models and improve our understanding of magnetospheric dynamics.

[3] Despite the recent advances made by analyzing ground-based and space telescope observations, several fundamental questions remain unanswered regarding the size and location of the Jovian polar cap and the mapping of various polar auroral features. For example, the main auroral oval emissions at Jupiter are not associated with the open/closed flux boundary in the polar cap, as they are at the Earth, but are thought to be associated with the breakdown of plasma corotation in the middle magnetosphere [*Clarke et al.*, 2004]. In auroral images, the boundary between open and closed flux in the ionosphere is not well defined, though the region of open flux is generally thought to be small. Additionally, the mapping of high-latitude auroral features to equatorial source regions is highly uncertain because global field models are known to be inaccurate beyond ~30 $R_J$ (1 $R_J$ = 71,492 km). The purpose of this paper is to investigate the link between regions in Jupiter's equatorial magnetosphere and the polar aurora.

[4] In order to identify the magnetospheric sources of auroral features, we have mapped contours of constant radial distance from the magnetic equator to Jupiter's ionosphere by performing a flux equivalence calculation. This approach enables mapping of the dayside magnetopause, thereby establishing possible locations of a portion of the open/closed flux boundary in Jupiter's polar cap. The mapping results should be useful in understanding models of dynamics and the open or closed nature of the Jovian magnetosphere.

[5] This paper is organized as follows. In section 2, we summarize the available auroral observations and the out-

[1]Institute of Geophysics and Planetary Physics, UCLA, Los Angeles, California, USA.
[2]Department of Earth and Space Sciences, UCLA, Los Angeles, California, USA.
[3]Department of Atmospheric, Oceanic, and Space Sciences, University of Michigan, Ann Arbor, Michigan, USA.
[4]LPAP, Institut d'Astrophysique et de Géophysique, Université de Liège, Liège, Belgium.


0148-0227/11/2010JA016148

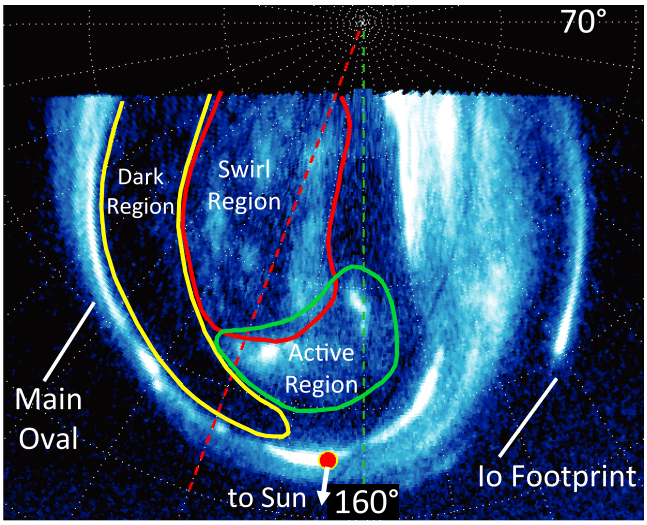


**Figure 1.** UV auroral emissions in Jupiter's northern hemisphere as imaged by the Hubble Space Telescope. The three polar auroral regions (active region, dark region, swirl region) have been labeled, and their locations for this particular time are delineated by the colored contours. This is a polar projection with CML 160°; the Sun's direction is indicated by the white arrow. Modified from Figure 5 of *Grodent et al.* [2003b].

standing questions in the field and discuss the motivation for our work. In section 3, we describe the flux equivalence calculation we use to map the auroral features to their magnetospheric sources; in section 4, we present the mapping results; and in section 5, we compare the mapping to auroral observations and describe the size and location of Jupiter's polar cap. In section 6, we discuss the results in the context of current models of magnetospheric dynamics and suggest other applications for the mapping results. We conclude with a summary.

## 2. Background

### 2.1. Main Oval Emissions

[6] The main oval emissions at Jupiter fall in a relatively constant, narrow (1°–3° latitudinal width) band that is fixed with respect to System III longitude [*Grodent et al.*, 2003a]. In the northern hemisphere, the main emissions are not actually shaped like an oval but display a kidney bean shape due to a "kink" that is also fixed in longitude; this shape can be seen in Figure 1, which is a polar projection of the UV auroral emissions in the northern hemisphere. The main emissions in the southern hemisphere are more oval shaped. A recent study [*Grodent et al.*, 2008b] revealed several morphological variations in the main oval as a function of local time: the dawnside portion forms a narrow arc, the postnoon portion consists of auroral patches, and the dusk portion appears to broaden and break from the main oval. Additionally, there is a discontinuity, believed to map to the prenoon local time sector, where the brightness is less than ~10% of the main oval brightness [*Radioti et al.*, 2008a]. Therefore, it was suggested that the term "main oval" should be replaced by the term "main emission." In both the UV and the visible domains, the main oval emissions may be accompanied by a fainter and variable secondary arc poleward of the main oval [*Pallier and Prangé*, 2001; *Vasavada et al.*, 1999]. Quasi-parallel arcs are also seen in the diffuse emissions located equatorward of the main oval on the dusk side, which have been attributed to electron scattering by whistler mode waves [*Radioti et al.*, 2009].

[7] The Jovian main auroral emissions are not believed to be associated with magnetospheric interaction with the solar wind but instead with the breakdown of plasma corotation in the middle magnetosphere. Plasma from the Io torus diffuses radially outward through flux tube interchange and must decrease its angular velocity in order to conserve angular momentum. Because the field is frozen into the flow, field lines in the magnetosphere are swept back azimuthally as the plasma's angular velocity decreases. A current system develops that features a field-aligned current coming out of the ionosphere on L shells beyond ~20, an outward radial current in the equator, and a returning field-aligned current into the ionosphere at larger L. The upward (out of the ionosphere) field-aligned current is carried by downward moving accelerated electrons that produce the main oval emissions. In the equatorial plane, the radial current provides a $\mathbf{j} \times \mathbf{B}$ force in the direction of corotation, increasing the azimuthal velocity of the plasma back toward corotation.

[8] Several theoretical studies have supported the view that corotation breakdown drives the main emissions at Jupiter. *Cowley and Bunce* [2001] used simple data-based models of the plasma velocity and north-south magnetic field component to calculate the magnitude of outward field-aligned currents in the middle magnetosphere. Inside of ~20 $R_J$ they represented the equatorial $B_z$ as an axisymmetric dipole with a contribution from a current sheet model [*Connerney et al.*, 1981], and outside of ~20 $R_J$ they represented $B_z$ as a function of radial distance based on a fit to Voyager 1 data [*Khurana and Kivelson*, 1993]. They found that the field-aligned currents associated with the breakdown of corotation peaked at radial distances of ~30–50 $R_J$ in the magnetosphere and that these currents map to a magnetic colatitude of ~16°, roughly consistent with the observed location of the main emissions. However, they also concluded that a field-aligned potential drop would be required to accelerate the electrons to high enough energies to drive the aurora. *Hill* [2001] performed a similar calculation under slightly different assumptions regarding the plasma rotational velocity [*Hill*, 1979]; he similarly concluded that the upward (out of the ionosphere) field-aligned current would be largest at $L = 30$ and that the main oval emissions could therefore be expected to map to ~30 $R_J$.

[9] These theoretical arguments have been supported by observations. For example, the discontinuity in the main oval brightness appears to map to a local time region where the field-aligned current reverses direction and flows downward into the ionosphere [*Radioti et al.*, 2008a; *Khurana*, 2001]. This downward current does not require that magnetospheric electrons be accelerated along the field, thus decreasing the brightness of the main oval in this region.

### 2.2. Satellite Footprints

[10] Auroral emissions have been observed at the footprints of Io, Ganymede, and Europa [*Connerney et al.*,

1993; *Clarke et al.*, 2002]. The satellite footprints are useful for constraining global field models because the satellites' orbital locations are known and a footprint's ionospheric location can therefore be linked reliably to a radial position in the magnetosphere. The longitudinal position can also be inferred, although with some small uncertainty as a consequence of the signal propagation time between the satellite and Jupiter's ionosphere. Thus, satellite footprints provide a check for field model accuracy at the orbital distances of Io (5.9 $R_J$), Europa (9.4 $R_J$), and Ganymede (15 $R_J$), and as a result, one can confidently map from the inner magnetosphere to the ionosphere.

[11] The VIP4 field model [*Connerney et al.*, 1998] was developed to match the Voyager 1 and Pioneer 11 magnetic field observations and to ensure that the model field lines traced from 5.9 $R_J$ matched the Io footprint in the ionosphere. The model does a good job of fitting the Io footprint, except in the auroral kink sector that gives the Io footprint its characteristic kidney bean shape. Recently, *Grodent et al.* [2008b] showed that addition of a magnetic anomaly in the northern hemisphere can improve the agreement between the model and footprint observations in the northern hemisphere, especially in the kink sector.

[12] Even with recent improvements such as the inclusion of a magnetic anomaly, the available field models are still accurate only within distances of ~30 $R_J$ in the equatorial plane. Beyond these distances, there are no satellite footprints to constrain the field models, and azimuthal currents stretch field lines and compromise the mapping. Some global magnetic field models [*Khurana*, 1997; *Alexeev and Belenkaya*, 2005] have incorporated these currents, although these models also have limitations. For example, the *Khurana* [1997] model did not include the effects of magnetopause currents, meaning that the model cannot be used in the dayside outer magnetosphere. The *Alexeev and Belenkaya* [2005] model includes the magnetopause current but neglects the dawn-dusk asymmetry of the equatorial magnetic field and presents the field configuration for a 0° dipole tilt and a 100 $R_J$ subsolar standoff distance. Both models were based on magnetic field data from a limited number of spacecraft flybys.

### 2.3. Polar Aurora

[13] We turn now from the satellite footprints, whose ionospheric positions can be mapped to the magnetosphere with a high level of confidence, to the highly variable and mysterious polar auroral emissions, whose magnetospheric mapping is uncertain.

[14] Based on the average brightness and temporal variability, the northern hemisphere UV polar emissions can be organized into three regions: the active, dark, and swirl regions [*Grodent et al.*, 2003b]. Their shapes and locations vary with time and as Jupiter rotates (see *Grodent et al.* [2003b], Figure 5, for an example of how the three regions shift). In the next few paragraphs, we will describe these three regions, which are illustrated and labeled in Figure 1, and the current theories of their magnetospheric sources.

[15] The active region is very dynamic and is characterized by the presence of flares, bright spots, and arc-like features. It is located just poleward of the main oval and maps roughly to the noon local time sector. There have been several interpretations of this region. *Pallier and Prangé* [2001] suggested that the bright spots of the active region are the signature of Jupiter's polar cusp, or possibly dayside aurora driven by an increase in the solar wind ram pressure. *Waite et al.* [2001] used the magnetohydrodynamic model of *Ogino et al.* [1998] to map an observed polar flare to near the cushion region, ~40–60 $R_J$ in the morning sector, and postulated that the flare could be produced by a magnetospheric disturbance due to a sharp increase in the solar wind dynamic pressure. Alternately, *Grodent et al.* [2003b] interpreted the polar flares as the signature of "explosive" magnetopause reconnection on the day side, based on their approximately minutes-long characteristic time scale. They also suggest that the arc-like structures could be the signature of a Dungey cycle dayside X line, following the arguments of *Cowley et al.* [2003].

[16] The dark region is located just poleward of the main oval in the dawn to prenoon local time sector. As its name suggests, the dark region is an area that appears dark in the UV, displaying only a slight amount of emission (0–10 kR) above the background level [*Grodent et al.*, 2003b]. In comparison, the main oval brightness is typically 50–500 kR [*Grodent et al.*, 2003a], and the active region flares have a brightness of a few hundred kilorayleighs [*Grodent et al.*, 2003b]. The dark region displays a crescent shape that contracts and expands as Jupiter rotates but appears fixed in local time [*Grodent et al.*, 2003b]. The jovicentric location of the dark region roughly matches the area where *Pallier and Prangé* [2001] observed faint inner ovals, or arcs; the most poleward arcs are roughly aligned with the poleward edge of the dark region. *Pallier and Prangé* [2001] suggested that these arcs map to closed field lines in the outer magnetosphere (out to ~70 $R_J$ based on the VIP4 model).

[17] Other interpretations of the dark region turn to models of global magnetospheric dynamics to explain the observations. For example, *Grodent et al.* [2003b] associated the UV dark region with the rotating dark polar region (r-DPR) [*Stallard et al.*, 2003], an area of subcorotating ionospheric flows, as measured by the Doppler shifts of infrared emission spectra. The dawnside r-DPR, and thus the dark region, is thought to be linked to the Vasyliūnas cycle [*Vasyliūnas*, 1983] return flow of depleted flux tubes [*Cowley et al.*, 2003]. In the Vasyliūnas cycle [*Vasyliūnas*, 1983], mass-loaded flux tubes are stretched as they rotate into the night side; they eventually pinch off, and reconnection occurs in the midnight-predawn local time sector, releasing a plasmoid that can escape down the tail, while empty flux tubes rotate back around to the day side. Similarly, *Southwood and Kivelson* [2001] argued that the main oval emissions map to the plasma disk, which would mean that the dark region, just poleward of the main oval, maps to the cushion region. The cushion region is an area of southward oriented and strongly fluctuating field in the outer magnetosphere in the postdawn to noon local time sector where the field becomes more dipole like than in the inner magnetosphere. It has been associated with empty flux tubes that were emptied by Vasyliūnas-type reconnection as they rotated through the night side [*Kivelson and Southwood*, 2005].

[18] The swirl region is an area of patchy, ephemeral emissions that exhibit turbulent, swirling motions. The swirl region is located poleward of the active and dark regions and is roughly the center of the polar auroral emissions. It is

generally interpreted as mapping to open field lines. *Pallier and Prangé* [2001] interpreted the area poleward of their inner arcs as being analogous to a polar cap for Jupiter; this area roughly matches the location and shape of the swirl region. In comparing the UV and IR observations, *Grodent et al.* [2003b] associated the UV swirl region with the fixed dark polar region (f-DPR), an area in which the ionospheric flows are nearly stagnant in the magnetic pole reference frame [*Stallard et al.*, 2003]. The stagnant flows in the f-DPR (swirl region) then suggest that the area maps to open field lines associated with Dungey cycle return flows [*Cowley et al.*, 2003], which are expected to flow across the ionosphere slowly because the Jovian magnetotail, is approximately hundreds or thousands of Jovian radii in length.

[19] An additional feature of the polar auroral emissions is the presence of transient spots located at the equatorward edge of the dark region. Because of their location, emitted power, and periodic recurrence, these polar dawn spots have been associated with the internally driven reconnection process and especially with the inward moving flow initiated during reconnection [*Radioti et al.*, 2008b, 2010].

### 2.4. Outstanding Questions and Motivation for This Work

[20] Many questions regarding the nature and causes of Jupiter's auroral emissions remain unanswered, despite the advances made from over a decade of Hubble Space Telescope (HST) observations and complementary theoretical studies. One such question is the size and location of the open/closed flux boundary in the ionosphere. The extent to which Jupiter's polar cap is open to the solar wind is a question of particular importance because the answer will have consequences for our understanding of global magnetospheric dynamics at Jupiter. For example, if Jupiter's magnetosphere is closed, as suggested by *McComas and Bagenal* [2007], then one expects Jupiter's polar cap to be small (~10° across). *McComas and Bagenal* [2007] proposed that magnetic flux that is opened via dayside reconnection with the solar wind is closed by reconnection on the magnetopause, near the polar cusps, rather than by reconnection in the tail. However, if cusp reconnection is unable to close all of the flux opened on the day side, as *Cowley et al.* [2008] argued, and the magnetosphere is open, then Jupiter's polar cap would correspond to a more significant fraction of the area inside the main auroral oval. In the discussion above, we introduced the polar auroral swirl region, which observations suggest may be associated with the polar cap and open field lines [*Pallier and Prangé*, 2001; *Cowley et al.*, 2003; *Stallard et al.*, 2003]. If these interpretations are correct and the swirl region is indeed associated with open field lines, the question then becomes why this region is not aurorally dark.

[21] A related outstanding issue is how and to what extent the solar wind influences the main emission brightness and position. It has been predicted that solar wind compressions will decrease auroral emissions: the inward moving plasma will increase its angular velocity to conserve angular momentum, decreasing the strength of the field-aligned current system that drives the main auroral emissions [*Cowley and Bunce*, 2001; *Southwood and Kivelson*, 2001]. Several studies have used spacecraft, such as Ulysses, Cassini, and New Horizons, as upstream solar wind monitors when examining the auroral response in both the IR and UV to changing solar wind conditions. For example, *Baron et al.* [1996] observed fluctuations in the $H_3^+$ emission intensity on short time scales that correlated well with the solar wind dynamic pressure as measured by Ulysses during its Jupiter encounter. Additionally, *Gurnett et al.* [2002] found that the hectometric radio emission, measured by the Galileo plasma wave science instrument, and auroral extreme ultraviolet emissions, measured by the Cassini ultraviolet imaging spectrograph, increased at the same time that an interplanetary shock reached Jupiter. Simultaneous HST observations of the aurora and Cassini data of the upstream solar wind conditions showed that the auroral emissions brightened by a factor of ~2 during a period of changing solar wind dynamic pressure; however, it remains unclear whether the brightening was associated with the magnetospheric compression or with the magnetospheric expansion [*Nichols et al.*, 2007]. More recently, *Clarke et al.* [2009] compared HST auroral observations with a solar wind model [*Zieger and Hansen*, 2008] based on data propagated from 1 AU and used New Horizons measurements to decrease timing uncertainties of the propagated solar wind model. They found that the total auroral power increased in response to forward shocks but not reverse shocks and that auroral brightening due to dawn storms are independent of solar wind conditions. Nonetheless, it remains possible that some parts of the aurora respond to forward shocks and other parts respond to reverse shocks.

[22] Other unanswered questions include the following.

[23] 1. Where do the polar auroral features (active, dark, and swirl regions) map to in radial distance and local time in the equatorial plane?

[24] 2. Do the main oval emissions map to similar equatorial radial distances at all longitudes?

[25] 3. What are the magnetospheric sources of the multiple auroral arcs? Where do they map, and what processes produce them?

[26] To address these questions, we have mapped contours of constant radial distance from the magnetic equator into the ionosphere. To accomplish this mapping, we performed a flux equivalence calculation, outlined in section 3, rather than tracing field lines from a model. Our method allows us to relate auroral features to their magnetospheric sources at a large range of radial distances and local times, a result that was previously inaccessible due to the lack of field models accurate beyond ~30 $R_J$. For example, we provide a reliable mapping of the three polar auroral regions, improving on the current models, which are only able to infer that the polar aurora emissions map to equatorial regions beyond ~30–50 $R_J$ because they lie poleward, of the main oval. We also are able to map the location of the dayside magnetopause, thereby establishing possible locations of a portion of the open/closed flux boundary in Jupiter's polar cap.

## 3. Methods

[27] Our objective is to map auroral features to their magnetospheric sources. One approach to such a mapping is to trace equatorial magnetic field lines from the magnetosphere to the ionosphere, as is frequently done in studies of the terrestrial magnetosphere. However, that method

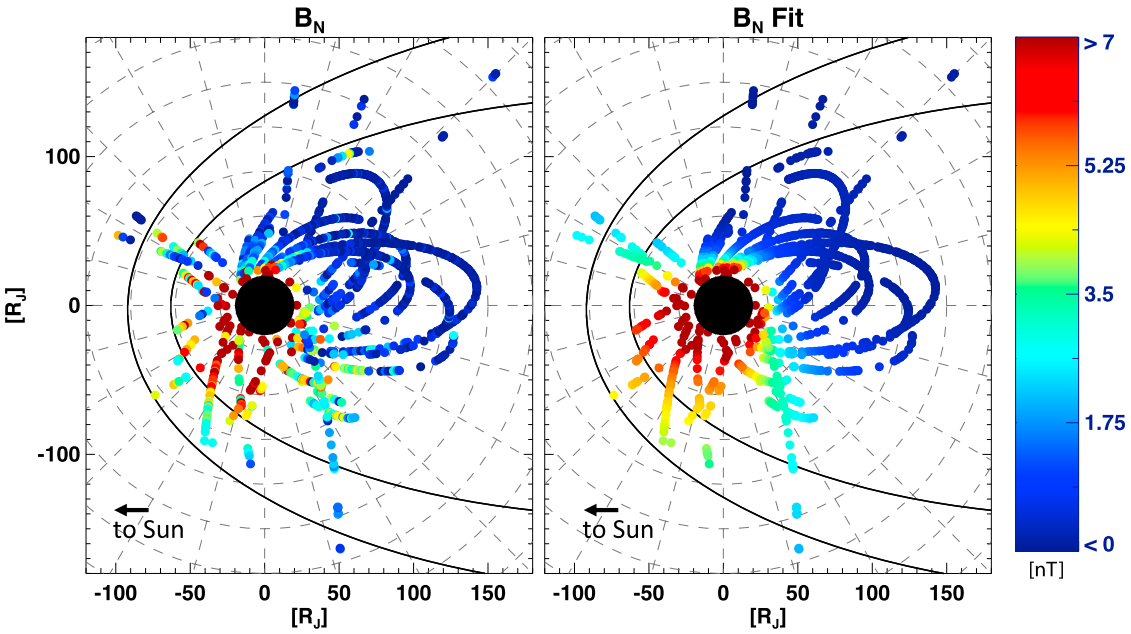


**Figure 2.** (left) Values for $B_N$ from spacecraft measurements and (right) equivalent values from a model fit plotted versus radial and local time in the equatorial plane. Probable magnetopause locations (one compressed, one expanded) are drawn in black [*Joy et al.*, 2002]. In both the data and the model, the field in the current sheet is strongest in the noon to dusk local time sector and weakest in the early morning.

requires an accurate global Jovian magnetic field model, and field models are highly uncertain at radial distances beyond ~30 $R_J$. The error arises, in part, because an azimuthal current flows through the equatorial plasma and stretches field lines at all local times. Though the available global field models are accurate only in the inner to middle magnetosphere, spacecraft observations of the magnetotail are available out to ~150 $R_J$, and we wished to consider auroral features that may map to the outer magnetosphere. We, therefore, took a different approach in our mapping. We started our mapping at the orbit of Ganymede, where the link to the auroral ionosphere can be determined from emissions identifiably linked to the moon. Thereafter, rather than following field lines along a field model, we mapped equatorial regions beyond Ganymede's orbit to the ionosphere by requiring that the magnetic flux threading a specified region at the equator must equal the magnetic flux in the area to which it maps in the ionosphere. Details of the procedure we used for the mapping follow.

### 3.1. Establishing the Radial and Local Time Dependence of the Equatorial $B_N$

[28] Measurements of the Jovian magnetic field are available at radial distances out to ~150 $R_J$ and at nearly all local times. Previous studies [*Khurana and Kivelson*, 1993; *Kivelson and Khurana*, 2002] have quantitatively described how $B_z$ falls with radial distance ($z$ is aligned with the spin axis and, on average, is normal to the current sheet), but little has been done to model changes with local time. Such changes are especially relevant for nightside modeling of $B_N$, the component of the magnetic field normal to the current sheet, which is known to be larger in the dusk hemisphere than in the dawn hemisphere.

[29] An important step in our mapping procedure is the calculation of the magnetic flux through the magnetic equator, which is a nonplanar surface in which the field magnitude reaches its minimum value along every flux tube. Calculation of the equatorial magnetic flux requires an accurate estimate of the average equatorial value of $B_N$, accounting for changes with radial distance and local time. We developed a two-dimensional model of the equatorial $B_N$ by fitting field measurements to a functional form that represents the dependence of the field on radial distance and local time. The data come from all spacecraft that have provided multiday measurements of the Jovian magnetic field: Pioneer 10, Pioneer 11, Voyager 1, Voyager 2, Ulysses, and Galileo. We restricted ourselves to data within 15° latitude of the jovigraphic equator, beyond 20 $R_J$, and with a time resolution of 24 s or better. To calculate $B_N$, we took 15 min running averages of $B_R$, $B_\theta$, and $B_\Phi$; interpolated the data to a time resolution of 8 s or better; and then, for each pass through the equatorial current sheet, we calculated the field magnitude from the three field components. Smoothing and interpolating the data in this fashion allowed us to more precisely identify $B_N$, defined as the minimum in the field magnitude during a current sheet crossing (within a few minutes of a $B_R$ and $B_\Phi$ reversal).

[30] In Figure 2, we have plotted the averaged $B_N$ values so determined (Figure 2, left) and the two-dimensional fit to those measured values (Figure 2, right) in the equatorial plane. Figure 2 indicates how $B_N$ varies with radial distance and local time. Figure 2 also shows the two most probable magnetopause locations (thick solid black lines) corresponding to a compressed and expanded magnetopause [*Joy et al.*, 2002]. The dayside magnetopause standoff distance is ~60 $R_J$ for the compressed magnetosphere and ~90 $R_J$ for

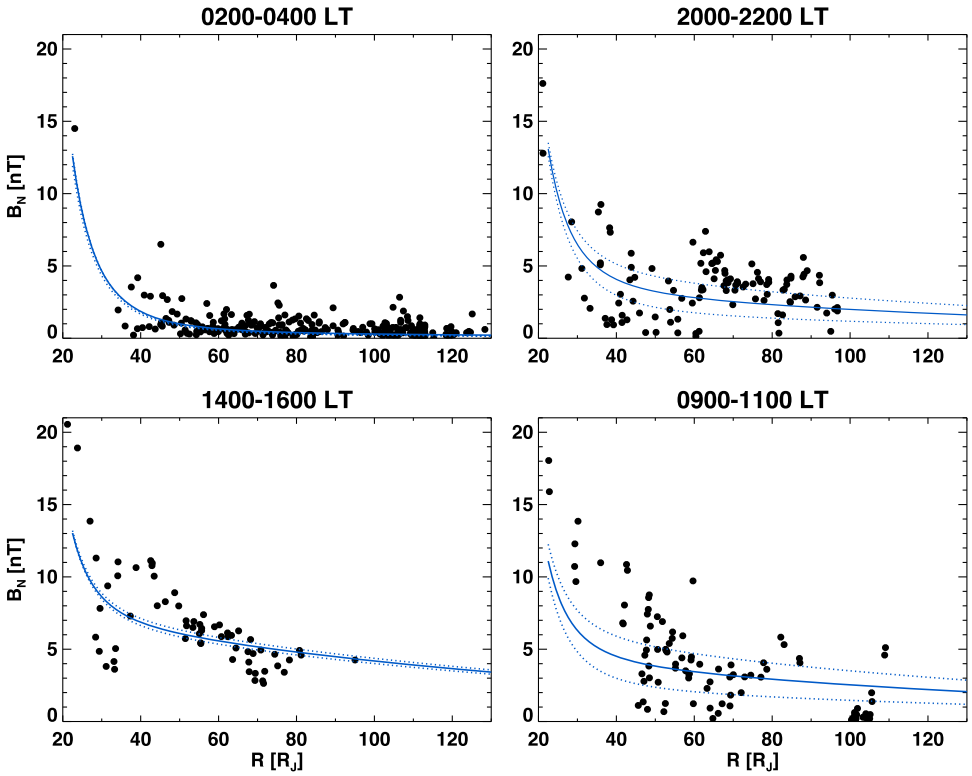


**Figure 3.** $B_N$ data (dots) and model (solid and dashed lines) as a function of radial distance for four local time bins. The solid lines indicating the model $B_N$ are taken for the median local time in each bin, with the dashed lines indicating how the model changes across each local time bin (i.e., for the 0200–0400 bin, the dashed lines are 0200 and 0400, and the solid line is 0300).

the expanded magnetosphere. In Figure 3, we have plotted the $B_N$ data (circles) and model (solid and dashed lines) as a function of radial distance for four different local time bins. The solid lines are taken for the median local time in each bin, with the dashed lines indicating how the model changes across each local time bin (i.e., for the 0200–0400 bin, the dashed lines are 0200 and 0400, and the solid line is 0300). Both Figures 2 and 3 show that the measured $B_N$ falls roughly exponentially with radial distance and is strongest in the noon to dusk local time sector (Figure 3, bottom left, 1400–1600 LT). The observations plotted here represent a range of solar wind and magnetospheric conditions, which could explain some of the variation in $B_N$ at a given position in the equatorial plane. For example, one expects the field strength to increase in response to a magnetospheric compression from the solar wind. Analogously, internally driven dynamics may influence the magnetospheric configuration [*Woch et al.*, 1998; *Kronberg et al.*, 2007].

[31] The fit was done using a routine that computes a nonlinear least squares fit to the data with a gradient-expansion algorithm. We assumed a functional form,

$$B_N(R,\varphi) = A\,R^{(B+C\cos(\varphi-D))} + [E + F\cos(\varphi - G) + H\cos(2\times(\varphi - I)) + J\cos(3\times(\varphi - K))] \times e^{-R/150}, \quad (1)$$

where $B_N$ is in units of nT; $R$ is the radial distance in $R_J$; $\varphi$ is the local time, measured from midnight, in radians; and $A$, $B$, $C$, $D$, $E$, $F$, $G$, $H$, $I$, $J$, and $K$ are constants that are determined by the fitting routine. Their values are provided in Table 1. This functional form was chosen to account for field changes with radial distance and local time, and to ensure that $B_N$ approaches zero as $R$ approaches infinity. The fit does a good job of reproducing the local time and radial dependences seen in the data; both the observed and model field are strongest near ~1500 LT (Figure 3, bottom left) and weakest in the post midnight sector (Figure 3, top left).

### 3.2. Mapping Using the Flux Equivalence Calculation

[32] As remarked above, rather than tracing field lines using a global field model, we have mapped from the equator to the ionosphere by means of a flux equivalence

**Table 1.** $B_N$ Fit Parameters

| Parameter | Value |
|---|---|
| A | 1.030e6 |
| B | −3.756 |
| C | −0.120 |
| D | 3.562 |
| E | 3.797 |
| F | −4.612 |
| G | 0.825 |
| H | 0.606 |
| I | 0.473 |
| J | 0.847 |
| K | 0.913 |

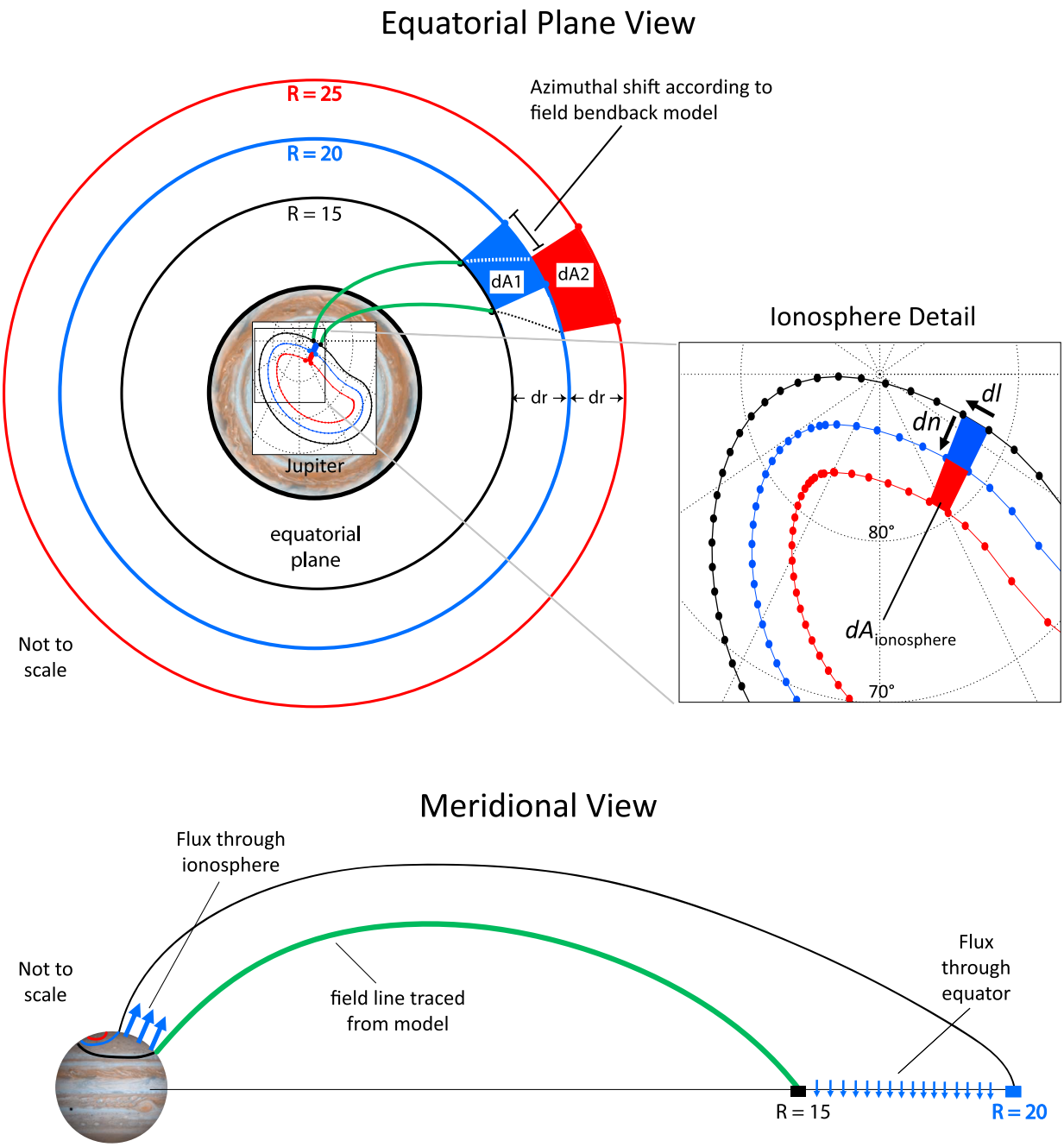


**Figure 4.** Illustration (not to scale) of the method used to map equatorial magnetic flux to the ionosphere by equating flux in the two regions. We begin by tracing along a field model from 15 $R_J$ in the equator, where the accuracy of the field model can be tested against observations of Ganymede's auroral footprint; this step is illustrated by the green lines. Next, we calculate the flux through the equator in the magnetosphere through a specified area pixel, labeled $dA_1$ here. We then determine how far to move the ionospheric boundary poleward, by solving for $dn$ according to equation (6). This gives us the mapping of a pixel linked to the 20 $R_J$ equatorial circle (in blue); further iterations of the calculation (illustrated in red) provide the mapping of successively distant equatorial circles.

analysis. A flux equivalence analysis has been used previously to estimate currents, flows, and magnetic mapping of Jupiter's ionosphere [*Cowley and Bunce*, 2001], although they used a simplified axisymmetric magnetic field model to estimate the magnetic flux. A key contribution of our work is that we calculate the magnetic flux using a two-dimensional databased $B_N$ fit that accounts for local time asymmetries. This will allow us to reliably map the source(s) of dawn-dusk

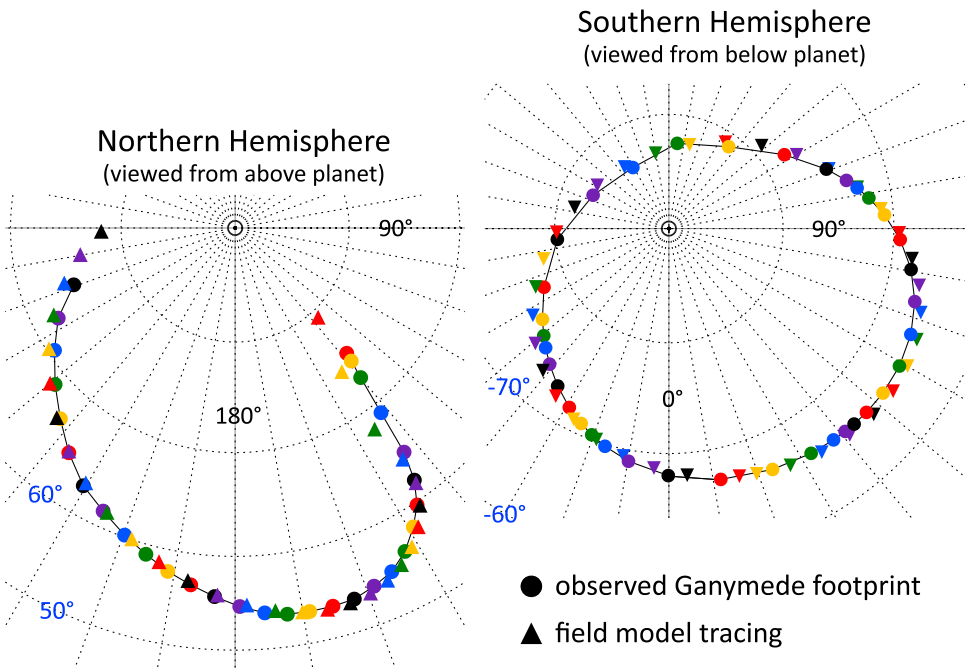


**Figure 5.** Comparison of the observed Ganymede footprint locations (circles) with the points where the model field lines traced from the location of Ganymede for successive observations reach the ionosphere (triangles). To guide the eye, the symbols are plotted in a repeating sequence of six colors (red, yellow, green, blue, purple, and black), rather than a continuous color bar. The observations (circles) should be compared to the closest mapped triangle of the same color, indicating that the equatorial longitude of Ganymede for a given observed footprint (circle) is the same as the initial equatorial longitude used in the field model tracing (triangle). The points are separated by 10° in longitude at the equator. For most points, the mapped ionospheric footprint comes close to matching the observed footprint.

asymmetries in the auroral emissions. In this section, we describe the calculation used to map from the equator to the ionosphere.

[33] To begin, we identified the ionospheric footprint of an equatorial circle at 15 $R_J$, the orbit of Ganymede and a distance where field models are reasonably accurate, by following model magnetic field lines from the equator to the ionosphere. This step is represented in Figure 4 by the solid green field lines, which connect the 15 $R_J$ equatorial curve (black circle) to the 15 $R_J$ ionospheric reference contour (black). In the northern hemisphere, we trace field lines from the field model of *Grodent et al.* [2008b], described above in section 2.2. This field model uses a version of the VIP4 plus current sheet model [*Connerney and Acuña*, 1998] with modified Schmidt coefficients and the addition of a magnetic anomaly in the form of an additional dipole located close to the surface to improve the agreement between the model and the satellite footprints in the northern hemisphere. Since the model is underconstrained, *Grodent et al.* [2008b] presented two possible solutions for the location and orientation of the perturbation dipole; we have used the one poleward of the Io footpath. For mapping to the southern hemisphere, we used the VIP4 plus current sheet model [*Connerney and Acuña*, 1998] with the original (unmodified) Schmidt coefficients, rather than the modified VIP4 model with magnetic anomaly, which had been constructed without regard to how the northern magnetic anomaly might affect the field in the southern hemisphere.

[34] We have a high level of confidence in the accuracy of our 15 $R_J$ reference contour because it matches observations of Ganymede's auroral footprint. Figure 5 presents the positions where the traced model field lines reach the ionosphere (triangles) and the observed locations of Ganymede's footprint (circles) for comparison. The footprint data for the northern hemisphere come from *Grodent et al.* [2008b, Table 1], and for the southern hemisphere, the data come from the same set of HST FUV images acquired with the Space Telescope Imaging Spectrograph (STIS) and Advanced Camera for Surveys SIII (ACS) instruments. The points are separated by 10° in longitude in the equator. To guide the eye, the symbols are plotted in a repeating sequence of six colors: red, yellow, green, blue, purple, and black. For the observations (circles), the color used in the plot indicates the longitude of the satellite at the equator. For the model results (triangles), the color indicates the initial equatorial longitude used in tracing the model field lines from the equator to the ionosphere. The observations should be compared to the closest mapped triangle of the same color.

[35] At most longitudes, the point obtained by tracing the field model falls close to the observed footprint. The largest errors in the northern hemisphere are at the extreme ends of the curve defined by the footprint path, and for all points but one, the model (triangles) falls at

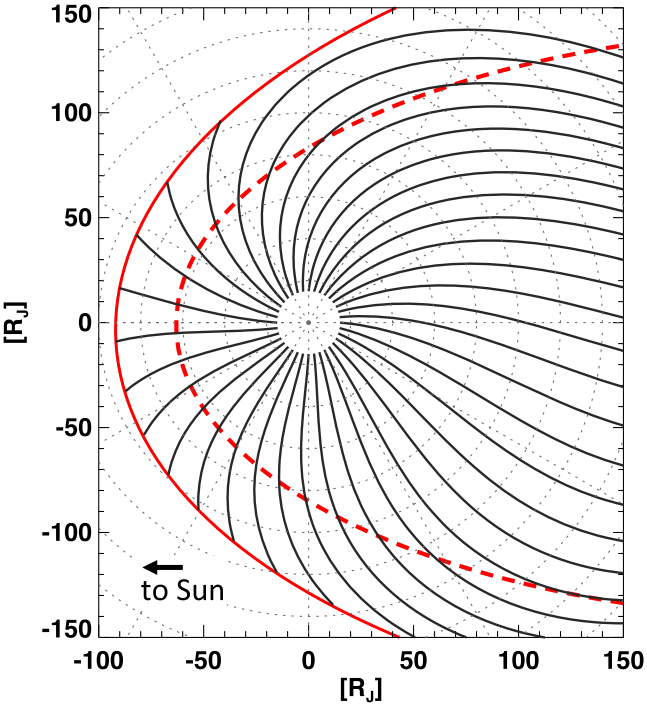


**Figure 6.** Field bendback model, projected into the equatorial plane, based on a fit to the data presented by *Khurana and Schwarzl* [2005]. Field lines are the most bent back near dawn and are bent forward near dusk. Two probable magnetopause locations are drawn in red [*Joy et al.*, 2002].

larger System III (SIII) left-handed longitudes than the observed footprint locations (circles). In both hemispheres, the error is mostly in the direction along the curve rather than in the latitudinal direction. However, as demonstrated by *Bonfond et al.* [2009], in the case of the Io footprint, most of this longitudinal shift cannot be attributed to the propagation time delay of the Alfvén waves. They suggested that the shift was due to inaccuracies of the magnetic field models. Such inaccuracies of the internal field models essentially affect our local time mapping with an estimated average local time error of ~0.7 h, and a maximum of ~1.6 h, although we can be confident in the validity with which radial distance and ionospheric latitude are linked.

[36] The next step was to calculate the equatorial magnetic flux for pixels of radial increment 5 $R_J$ and an initial longitudinal width of 5–15°. The pixels' azimuthal width was allowed to vary in order to ensure that the ionospheric pixels were relatively evenly spaced. The schematic illustration of Figure 4 explains the approach used (not to scale). In Figure 4, a typical pixel in the equator, labeled $dA_1$, is drawn in blue. The flux through the equator is given by

$$d\Phi_{equator} = B_{N,equator}(R,\varphi)\cdot dA_{equator}, \quad (2)$$

where the normal component of the magnetic field at the equator, $B_{N,equator}$, is a function of radial distance $R$ and local time $\varphi$ given by the fit of equation (1). We approximate the equatorial flux by

$$d\Phi_{equator} = B_{N,equator}(R,\varphi)R\,dr\,d\varphi. \quad (3)$$

In the mapping from 15 to 20 $R_J$, no shifts in local time were used. At larger radial distances, the equatorial pixels were shifted azimuthally in the equator according to a simple field bendback model. We developed this field bendback model using a simple functional form to fit measured $B_R$ and $B_\phi$ values, again using the nonlinear least squares fitting procedure. The data used in the fit are the same as those shown in Figure 8 from the study by *Khurana and Schwarzl* [2005]. Our field bendback model is shown in Figure 6, where we have plotted the field line projections onto the equatorial plane. This field bendback model varies with both radial distance and local time, and, as a result, the equatorial area pixels do not have a fixed longitudinal width. The bendback model reproduces the data well and includes a strongly bent back field in the postmidnight sector and a bent forward field in the dusk local time sector. We have illustrated the effects of including the field bendback in Figure 4, where the dashed black and white lines between 15 and 20 $R_J$ represent the field bendback in the equatorial plane and dictate how two pixels at the same local time in the equator can be found misaligned in the ionosphere. Because the bendback changes with longitude, the azimuthal widths of area elements $dA_2$ and $dA_1$ may differ.

[37] After evaluating the equatorial magnetic flux through a typical pixel, we matched the ionospheric flux by moving along a normal to the ionospheric reference curve. Equating the equatorial magnetic flux with the ionospheric flux determines how far poleward we should place the auroral boundary of each ionospheric pixel to obtain the ionospheric mapping of the 20 $R_J$ circle at the equator. This poleward distance, which we call $dn$ (Figure 4, top, inset), is determined by the flux equivalence calculation as follows: the ionospheric magnetic flux is given by

$$d\Phi_{ionosphere} = B_{R,ionosphere}(R = 0.95\,R_J,\theta,\varphi)\cdot dA_{ionosphere}, \quad (4)$$

where $\theta$ and $\varphi$ are the colatitude and azimuthal angle in spherical coordinates, respectively. We estimate the radial component of the ionospheric field, $B_{R,\mathrm{ionosphere}}$, using the same internal field models (different for north and south) used for mapping the 15 $R_J$ circle to the ionosphere. The ionospheric area element, $dA_{ionosphere}$, is computed as the product of $dl$, the length in the direction along the ionospheric contour, and $dn$, the length in the poleward direction to be determined (Figure 4, top, inset). Following *Grodent et al.* [2008b], we used a sphere of radius 0.95 $R_J$ to approximate Jupiter's oblate surface (~0.935–0.9585 $R_J$) over the range of latitudes (90° to ~53°) of interest in the northern hemisphere. For consistency, we also use a sphere of radius 0.95 $R_J$ when calculating the flux through the southern hemisphere. This approximation introduces a negligible (less than 1%) error in the calculated flux at the surface, though for certain specific applications, mapping to a different reference surface may be required.

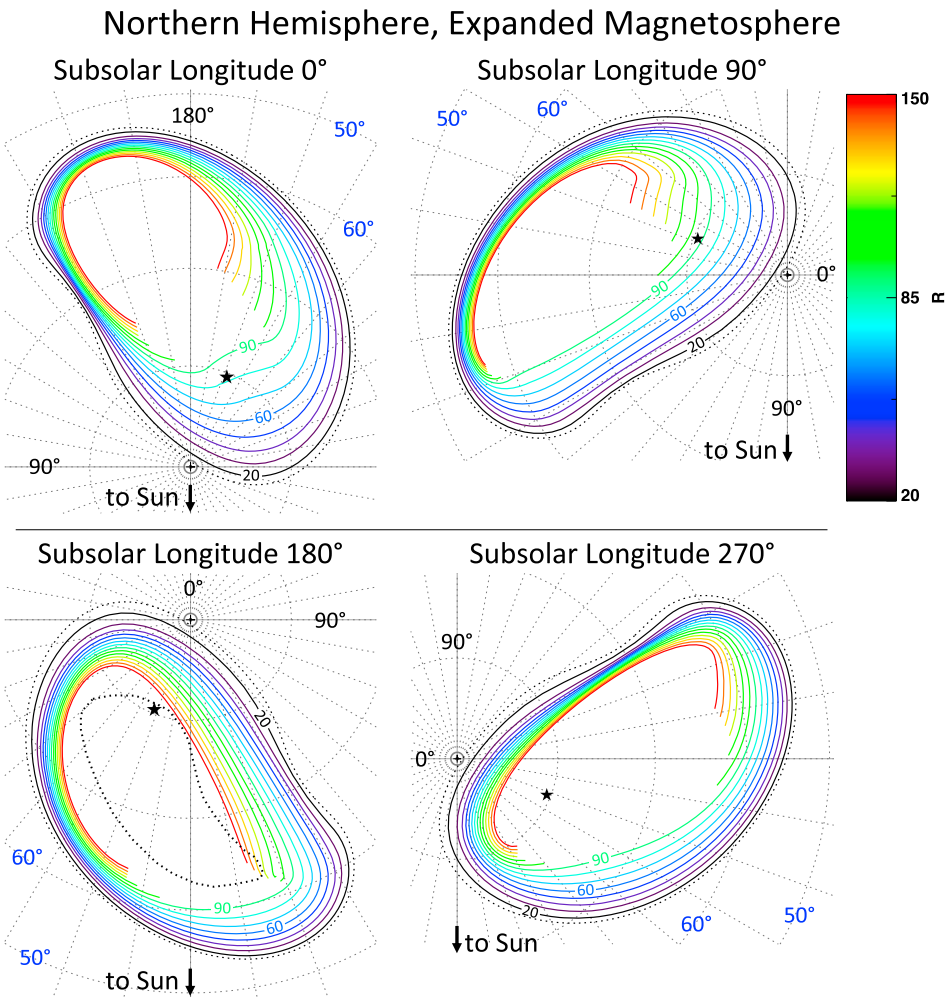


**Figure 7.** Polar view of the flux mapping results for the expanded magnetosphere (dayside magnetopause standoff distance of ~90 $R_J$) for four different viewing orientations. Local noon is indicated by arrows and is in the same direction for all four panels; dawn is to the left, and dusk is to the right. Contours are colored to indicate the equatorial radial distances to which they map, ranging from 20 $R_J$ (solid black) to 150 $R_J$ (red) in 10 $R_J$ increments. The outer dashed black line is the 15 $R_J$ reference contour, which matches the Ganymede footprint. In all four panels, the contours are closer together on the left/top left side, which maps roughly to the postmidnight to dawn local time sector, than on the right side, which maps roughly to the noon to dusk sector. This is expected because the equatorial $B_N$, and thus the magnetic flux through the equator, is strongest in the postnoon to dusk local time sector. Black stars indicate the location of the magnetic pole, at 9.6° colatitude and 212° SIII longitude. All four panels are plotted on the same scale.

[38] We can approximate equation (4) as

$$d\Phi_{ionosphere} = B_{R,ionosphere}(R = 0.95\,R_J, \theta, \varphi) \cdot dn\,dl. \quad (5)$$

Finally, we set $d\Phi_{equator} = d\Phi_{ionosphere}$, and solve for $dn$

$$dn = \frac{B_{N,equator}\left(R_{equator}, \varphi_{equator}\right) R\,dr\,d\varphi}{B_{R,ionosphere}(R = 0.95, \theta, \varphi)\,dl}. \quad (6)$$

It is this final calculation that gives us the location of a portion of the ionospheric contour corresponding to the 20 $R_J$ circle at the equator (Figure 4, blue curves).

[39] Iteration of the calculation provides the ionospheric mapping of successively distant circles (illustrated in Figure 4 by the red curves representing the mapped 25 $R_J$ equatorial circle). We continue the flux equivalence calculation out to a radial distance of 150 $R_J$, the limit of the magnetic field data coverage in the magnetotail and the valid region of our $B_N$ fit. However, the Jovian magnetotail is estimated to extend for thousands of $R_J$ [*Lepping et al.*, 1983], so we have mapped only a small fraction of the magnetotail. We expect that this omission will have only a minor effect on the results because the equatorial flux will be relatively small at distances beyond 150 $R_J$ and give quantitative arguments to that effect in section 5.2.

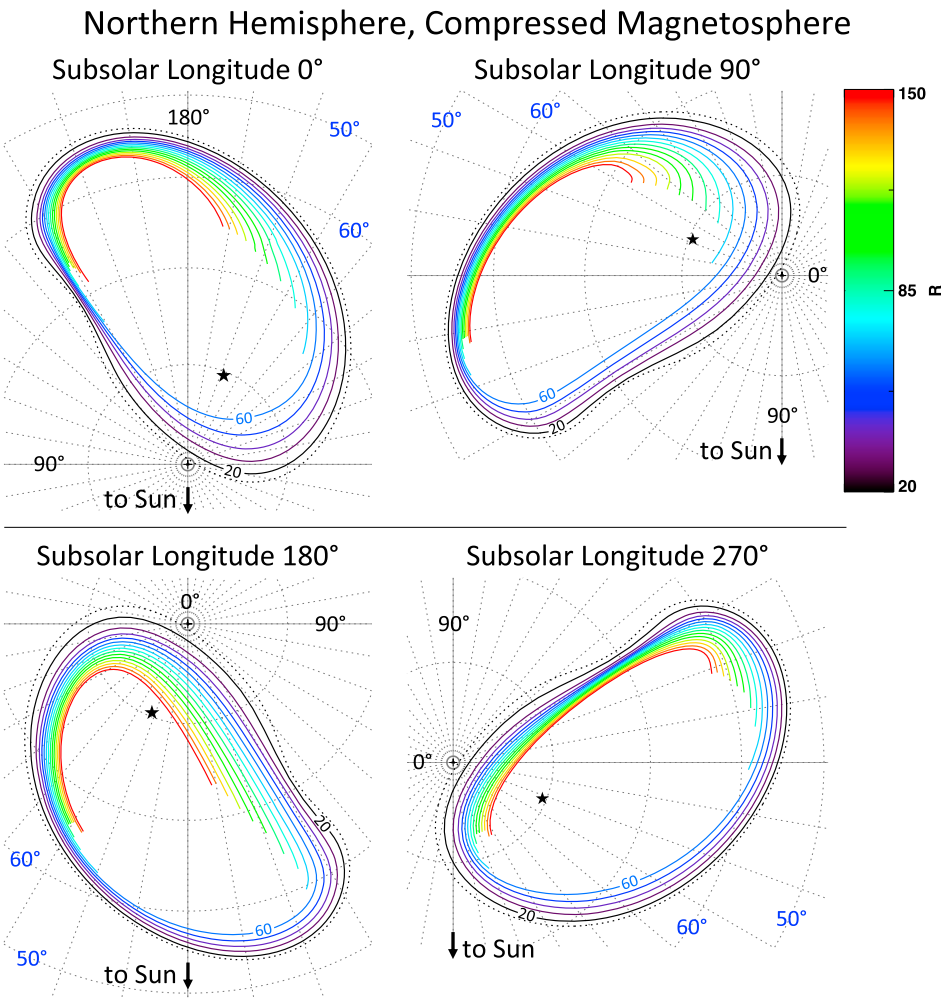


**Figure 8.** As in Figure 7 but for a compressed magnetosphere (dayside magnetopause standoff distance of ~60 $R_J$). The area of open flux, or the white area interior to the colored contours, is larger for the compressed magnetopause case than for the expanded magnetopause.

[40] Inspection of equation (6) shows that $dn$ is proportional to $B_{N,\text{equator}}$, which is itself a function of radial distance and local time. The variation of $B_{N,\text{equator}}$ with local time shown in Figure 2 makes it evident that the ionospheric contours mapping to a constant radial distance in the equator will have the largest separation in the ionosphere in the postnoon to dusk local time sector, where $B_{N,equator}$ attains its maximum value.

## 4. Results

[41] We have mapped the equatorial magnetospheric flux at radial distances between 20 and 150 $R_J$ into the ionosphere. The results depend on how the ionospheric region of interest is oriented with respect to the Sun, or local noon, because the flux equivalence calculation involves $B_N$, which is a function of local time. The effect of the orientation is familiar from images of the aurora at different central meridian longitudes (CMLs), i.e., the Jovian longitude facing the direction of the Earth. Therefore, in Figures 7–9 (northern hemisphere) and 10–12 (southern hemisphere), we present mapping results for four different viewing orientations, with local noon at 0°, 90°, 180°, and 270° SIII left-handed longitude. In Figures 7–12, we have plotted the contours corresponding to constant radial distances, every 10 $R_J$ from 20 $R_J$ to 150 $R_J$. The outermost black dashed line is the 15 $R_J$ reference contour, matching Ganymede's auroral footprint, obtained by tracing a field model as outlined in section 3.2.

[42] In Figures 7, 8, 10, and 11, we use color to represent the equatorial radial distance to which different portions of the auroral contours map, ranging from 20 $R_J$ (black) to 150 $R_J$ (red). In Figures 9 and 12, we use color to represent the equatorial local time to which different portions of the auroral contours map. The field lines to the left generally map to the morning and predawn sector, while field lines to the right generally map to the dusk sector. The contours of constant radial distance (10 $R_J$ equatorial separation) have the largest separation on the right (approximately dusk) side because of the local time asymmetry in the

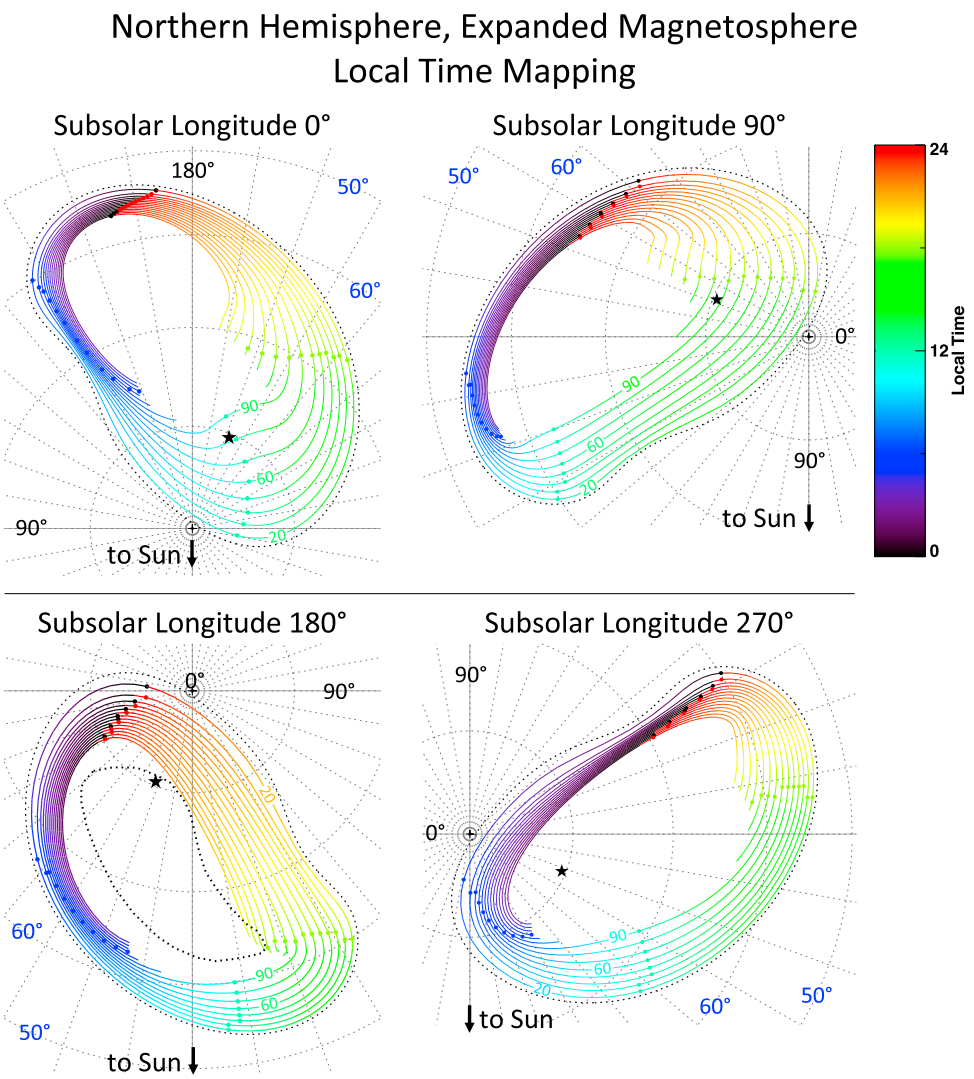


**Figure 9.** As in Figure 7, but the colors now indicate the equatorial local time mapping along the contour. The region on the left/top left side where the contours are closest together maps to the post-midnight to dawn local time sector (black to blue), where the equatorial $B_N$ is weakest. Small colored circles indicate the point closest to local midnight (red or black circles), dawn (dark blue), noon (blue-green), and dusk (light green/yellow).

equatorial $B_N$, which is strongest in the afternoon sector (Figure 2). As a result, the area of open flux is shifted toward the predawn to dawn side (left/top left).

[43] We terminate the contours where the field lines map to the magnetopause of *Joy et al.* [2002] (~60 $R_J$ at noon and ~85 $R_J$ at dawn/dusk for the compressed case and ~90 $R_J$ at noon and ~130 $R_J$ at dawn/dusk for the expanded case). The white or empty area interior to the colored contours maps beyond 150 $R_J$ on the night side and beyond the magnetopause on the day side; we interpret these areas as open flux and will justify this interpretation in section 6. The magnetopause lies closer to the planet for the compressed case than for the expanded case, and therefore the area of open flux is larger for the compressed magnetopause (Figures 8 and 11) than for the expanded magnetopause (Figures 7 and 10).

[44] When comparing the areas of open flux between the compressed and the expanded cases, it is important to note that we use the same flux equivalence calculation method and model $B_N$ field strength in both cases. The assumption that $B_N$ is not affected by displacement of the magnetopause is undoubtedly an oversimplification, as one would expect that the field strength would increase in response to a magnetospheric compression from the solar wind. For example, *Hanlon et al.* [2004] found that an interplanetary shock observed by Cassini during its approach to Jupiter produced an ~3 nT increase in the magnitude of $B_z$ (from an average magnitude of ~2–5 nT) as recorded by Galileo, inside the Jovian magnetosphere at ~60–80 $R_J$ and ~2000 LT. However, our model $B_N$ is itself an average of values relevant to all possible magnetopause locations, so it is not possible to correct consistently for changes of the size of

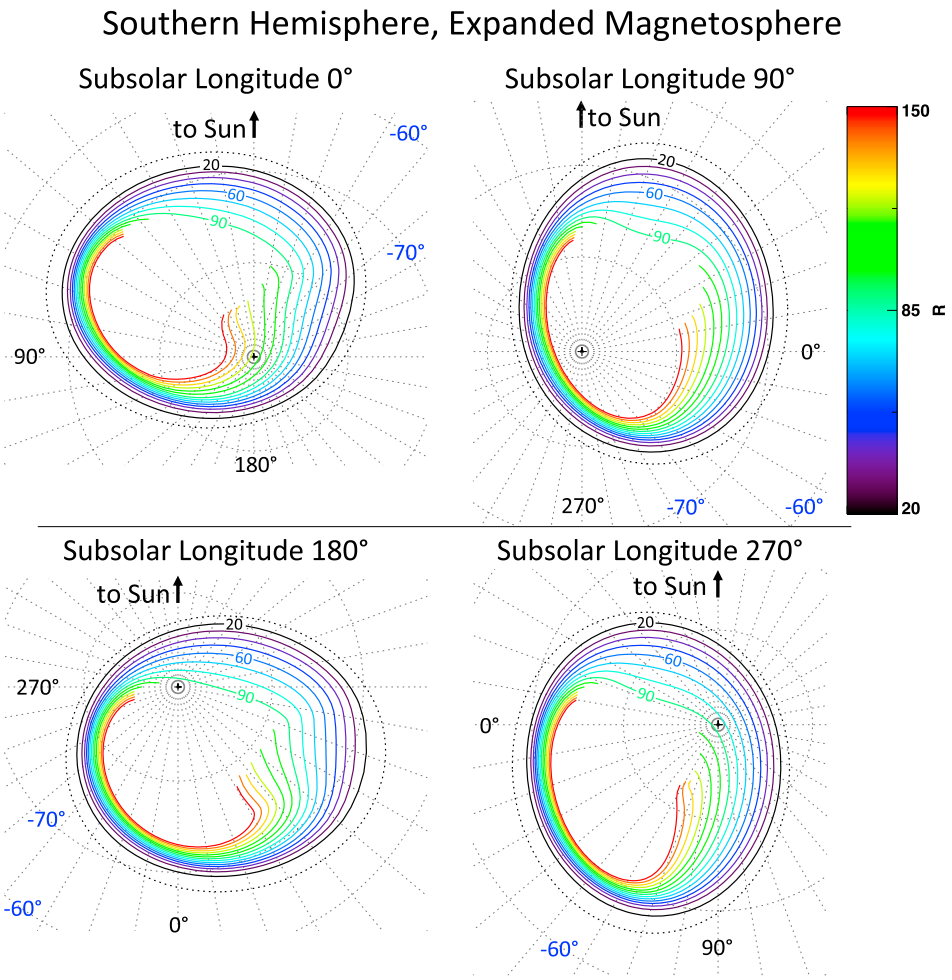


**Figure 10.** As in Figure 7 but for the southern hemisphere, as seen by an observer looking up at the planet. The Sun's direction is now toward the top of the page, dawn is to the left, and dusk is to the right.

the magnetosphere. As discussed in section 3.2, and as is evident from equation (6), the separation of the ionospheric contours, *dn*, is proportional to $B_N$. This means that if we underestimate $B_N$, for the compressed case, then we also underestimate *dn* and overestimate the area of open field lines; equivalently, we probably underestimate the area of open flux for the expanded case. As a consequence, the configurations we considered here can be seen as the extreme cases.

[45] Changes in the viewing orientation influence the mapping results, as can be clearly seen in the difference between subsolar longitude 0° and subsolar longitude 180° in the northern hemisphere. For both orientations, the ionospheric contours of constant radial distance are farthest apart near noon local time, where the equatorial field strength is the strongest, and are closest together at nightside local times, where the equatorial field strength is weakest. However, for subsolar longitude 0°, the spacing between contours on the day side is at least twice as large as for subsolar longitude 180°. Similarly, the nightside contours are much closer together for subsolar longitude 0° than for subsolar longitude 180°. This occurs because the ionospheric $B_R$ is not uniform, as can be seen in Figure 13. For subsolar longitude 180°, the ionospheric field in the region mapping near noon is at least 15 Gauss, while for subsolar longitude 0° the ionospheric field in the region mapping near noon is ~7 Gauss. Because *dn* is inversely proportional to $B_R$, the weak ionospheric field for subsolar longitude 0° means that the ionospheric contours near the day side will be farther apart for subsolar longitude 0° than for subsolar longitude 180°.

## 5. Analysis

[46] With models of the link between different magnetospheric regions and their magnetic footprints in the ionosphere established, it is of interest to compare the results to UV and IR auroral observations. The comparison can be used to describe the size and location of Jupiter's polar cap.

### 5.1. Comparison to Auroral Observations

[47] Auroral emissions in the UV provide a direct signature of magnetospheric particle precipitation [*Prangé et al.*, 2001]. Additionally, the typical spatial resolution of the HST UV auroral images taken with STIS is 0.024 arcsec/pixel [*Clarke et al.*, 2002], while the platescale of the

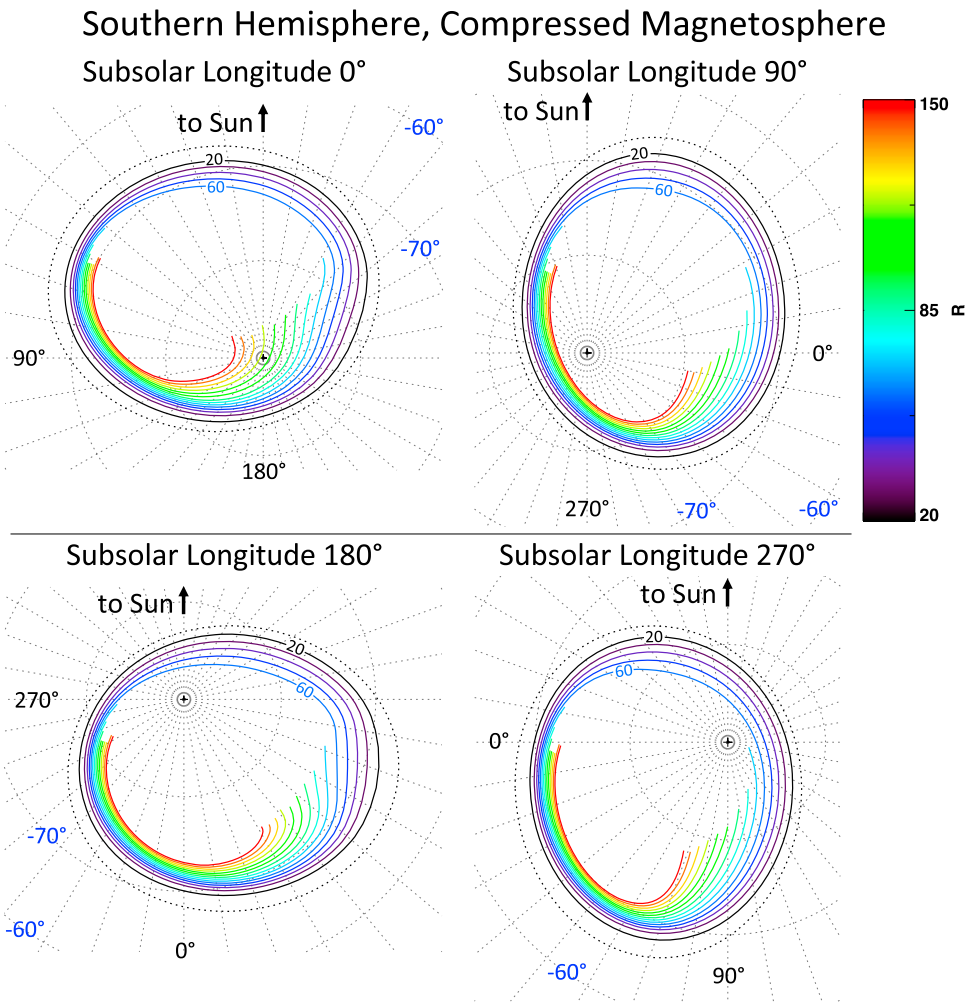


**Figure 11.** As in Figure 8 but for the southern hemisphere.

NSFCam instrument at the Infrared Telescope Facility is only 0.148 arcsec/pixel [*Satoh and Connerney*, 1999]. Therefore, in this section we focus our discussion on UV auroral emissions and only briefly discuss a comparison with the ionospheric flow patterns and resulting open/closed flux boundary inferred from IR auroral observations.

[48] As discussed in section 2.3, the UV polar auroral emissions can be categorized by their brightness, morphology, and temporal variability into three regions: the active, dark, and swirl regions. The shapes, sizes, and locations of the three polar regions vary with solar wind conditions and as the planet rotates; the mapping also varies (Figures 7–12). Therefore, in this section we will compare the mapped contours to UV auroral observations at two different CMLs, or the Jovian longitude in the direction toward the Earth. We will restrict the discussion to auroral observations in the northern hemisphere, for which more observations are available than for the southern hemisphere as a consequence of the viewing geometry [*Grodent et al.*, 2003b].

[49] In Figures 14a–14c and 15a–15c, we present our mapping results for two different viewing orientations, CMLs 160° and 220° SIII left-handed longitude, respectively, and in Figures 14d and 15d, we show the corresponding UV auroral observations (modified from Figure 5 in the study by *Grodent et al.* [2003b]). Figures 14a and 15a show mapping results for an expanded magnetopause and the contours colored to indicate the equatorial radial distance to which they map; Figures 14b and 15b show the same mapping results, but the colors indicate the equatorial local time mapping. Figures 14c and 15c follow the same format as Figures 14a and 15a but present mapping results for a compressed magnetopause. The Sun direction is indicated by black arrows.

[50] To facilitate comparison with the UV and IR auroral observations, we have added contours relating the auroral observations to our mapping results. *Grodent et al.* [2003b] drew contours delineating the active (green), dark (yellow), and swirl (red) regions in the polar aurora, as shown in Figures 14d and 15d. (These regions are also discussed in section 2.3.) In Figures 14a–14c and 15a–15c, we have overplotted the contours of *Grodent et al.* as thick curves at the same jovicentric coordinates to outline the three polar auroral regions (substituting black for yellow to outline the dark region). The inner dashed black contour in

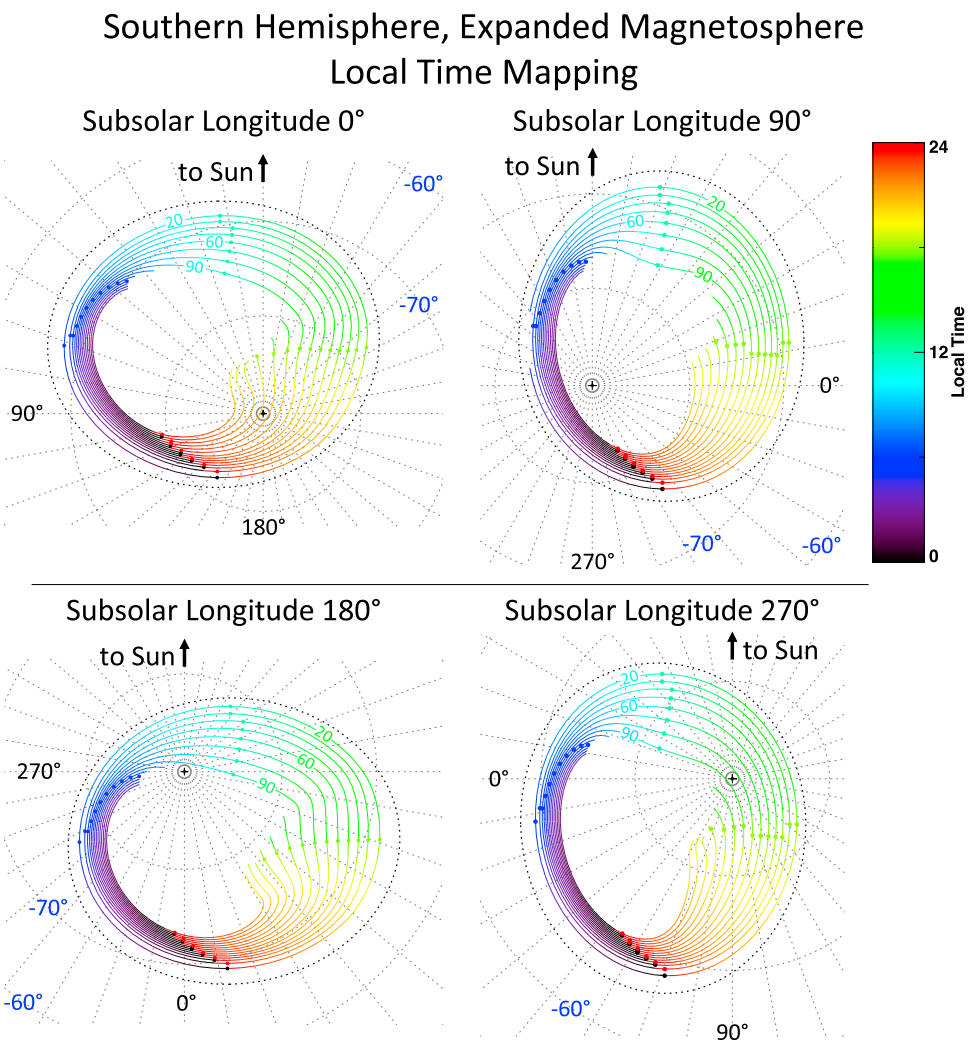


**Figure 12.** As in Figure 9 but for the southern hemisphere.

Figures 14a–14c is the jovicentric location of the fixed dark polar region from the IR auroral observations of *Stallard et al.* [2003]. As discussed in section 2.3, because of the stagnant flow within this region, it is believed to contain open field lines. The f-DPR location was derived from observations taken at CMLs of ~160° to ~180° and should only be compared to mappings representing similar CMLs (T. Stallard, personal communication, 2010). Therefore, we have not included it in Figure 15 (CML 220°).

[51] Figure 14 shows mapping results and auroral observations for CML 160°. In this orientation, the Sun direction is oriented to the bottom of the page and slightly to the right, as indicated by a black arrow. The auroral active region maps to field lines just outside the dayside magnetopause, plausibly open field lines in the polar cusp. The swirl region maps to tail field lines at distances larger than 150 $R_J$, plausibly open field lines; the *Stallard et al.* [2003] f-DPR lies within that region. The dark region maps to both open and closed field lines near dawn local time, and the degree to which it is on open field lines changes greatly between the compressed and uncompressed expanded cases. We will comment on this further in section 5. In Figure 14e, the composite of auroral observations and mapping results show that the main oval radial mapping changes with local time/longitude. The main oval maps to ~15–30 $R_J$ near dawn, ~30–50 $R_J$ near noon, and 50–60 $R_J$ at ~1500 LT.

[52] Figure 15 shows mapping results and auroral observations for CML 220°. In this orientation, the Sun is toward the bottom right, and one can see that the auroral emissions have rotated with the planet. Now the dusk local time sector maps roughly to the top right, whereas dawn local time maps roughly to the bottom left (Figure 15b). As in Figure 14, the boundaries of the auroral polar regions have been marked by the thick green (active region), black (dark region), and red (swirl region) lines.

[53] By comparing the UV observations for the two CMLs, we can see that the shapes and relative sizes of the polar regions shift as the planet rotates from CML 160° to CML 220°. For example, the active region (outlined in green) has become elongated in longitude and shifted

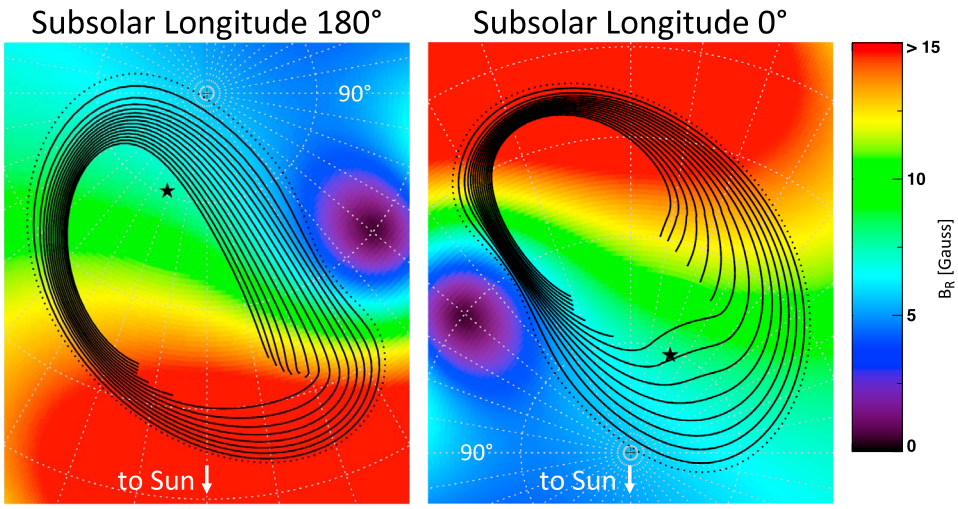


**Figure 13.** Ionospheric $B_R$ strength in the northern hemisphere, with mapping contours overplotted in black. The magnetic field is given by the model described in section 3.2. The direction of the Sun is indicated by the white arrows. For subsolar longitude 180°, the ionospheric field is strongest in the region that maps near local noon, where the equatorial field strength is also strongest. Half a Jovian rotation later, at subsolar longitude 0°, the ionospheric field is weakest in the region that maps near local noon. As a result, the ionospheric contours mapping near noon are farther apart for subsolar longitude 0° than for subsolar longitude 180°.

equatorward. Our mapping contours have also shifted in Figure 15 compared to the position and configuration shown in Figure 14. As a result, we find that the polar auroral regions map to generally the same magnetospheric region(s) for CML 220° as they did for CML 160°. The active region still maps to field lines just beyond the (compressed) dayside magnetopause boundary, though it maps to a wider range of local times, from slightly postdawn through dusk, than in Figure 14. The swirl region again maps to field lines on distances beyond 150 $R_J$. The dark region now maps almost entirely to field lines outside the dayside magnetopause or beyond 150 $R_J$ for both the compressed and expanded cases, whereas for CML 160° a portion of the dark region mapped to field lines within the dayside magnetopause or inside of 150 $R_J$. Whereas the dark region mapped to postmidnight to prenoon local times for CML 160°, it now maps roughly to the midnight to dawn local time sector. The main oval mapping again varies with local time, from ~20–30 $R_J$ near dawn to ~30–50 $R_J$ prenoon and ~50–60 $R_J$ postnoon.

[54] The auroral observations for CML 220° include two spots, one in the dawn sector and one nightside spot, that are thought to be the signature of magnetic reconnection in the tail [*Grodent et al.*, 2004]. The spot locations from Figures 15c and 15d are indicated in Figures 15a, 15b, and 15e by magenta ovals. However, because the spots are so close to the limb, their locations in the polar projection are subject to error because of stretching due to limb fitting. Taking this error into account, we find that the polar dawn spot maps to ~50–80 $R_J$ and ~0200–0400 LT and the nightside spot maps to ~50–90 $R_J$ and ~2100–2400 LT. That both spots map to equatorial regions planetward of the statistical X line supports the association with inward moving flow released during tail reconnection, as was shown by *Radioti et al.* [2010] for the polar dawn spots and recently by *Radioti et al.* [2011] for the nightside spots.

[55] On the basis of the above comparison with auroral observations, we interpret the polar auroral active region as forming Jupiter's polar cusp and the swirl region as Jupiter's polar cap. It is also clear that there are several ways in which to explain the absence of emissions in the dark region. Where the dark region maps to open field lines, the relative lack of auroral emissions can be explained by an exceptionally low plasma density. On closed field lines coupled to the dark region, one potential explanation for the relative lack of auroral emissions is the presence of downward (into the ionosphere) closure currents, analogous to the terrestrial black aurora that are also associated with downward field-aligned currents on closed field lines [e.g., *Marklund*, 2009]. Our interpretation is in line with the previous discussion of *Cowley et al.* [2003], who suggested that aurorally dark regions at Jupiter might be associated with either open field lines or downward (into the ionosphere) currents on depleted flux tubes as part of the Vasyliunas cycle return flow. In Figure 16, we present a schematic illustration of the relationship between polar auroral features and their magnetospheric sources. Figure 16 shows both closed (dark blue) and open (light blue) field lines emerging from the dark region, on either side of the open/closed flux boundary (dashed pink line). An open field line is also shown emerging from the swirl region, which we have interpreted as the polar cap. The active region is labeled as the polar cusp.

[56] Our flux equivalence calculation assumes an equatorial field value $B_N$ averaged over all solar wind and magnetospheric conditions, even though we have analyzed

our results for boundaries at locations consistent with high and low solar wind dynamic pressure. Our results, therefore, are not fully consistent with any specific solar wind condition. Nonetheless, in this section we have drawn comparisons to the polar auroral observations taken at a specific moment in time, under a specific set of solar wind conditions, and we cannot expect our model to represent the actual boundaries for those conditions. We expect that

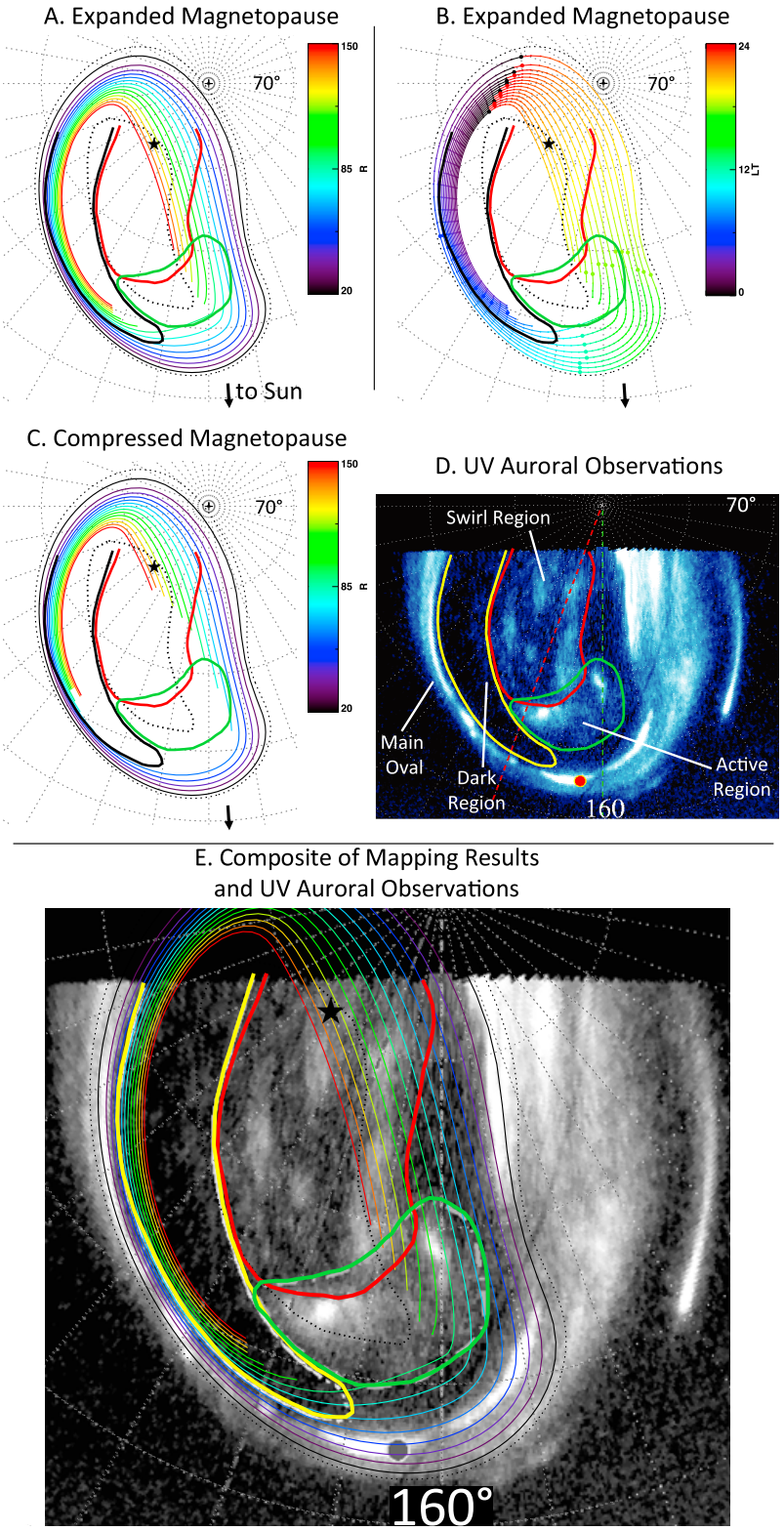


**Figure 14**

the shapes and locations of the three polar regions will change in time. This error is not expected to greatly affect our interpretation of the active and swirl regions, although we are less confident in our dark region mapping and interpretation because for one CML, the dark region maps partially inside 150 $R_J$, but for the other CML, it maps almost entirely beyond 150 $R_J$.

### 5.2. Size and Location of Jupiter's Polar Cap

[57] In section 5.1, we identified the polar auroral swirl region as the Jovian polar cap because it maps to lobe field lines beyond 150 $R_J$ that we believe to be open, in part because this region is characterized by extremely low density plasma, $<10^{-5}/\mathrm{cm}^3$ [*Gurnett et al.*, 1980]. In this section we will assume that most of the region beyond 150 $R_J$ in the tail and outside the dayside magnetopause are open and discuss in more detail the size and shape of the polar cap, to which the open flux maps in both the northern and southern hemispheres. We will also compare the flux through the polar cap to the estimated lobe flux based on spacecraft measurements in the magnetotail.

[58] Results of the flux equivalence calculation show that the region of open flux is skewed toward the dawn side. In both hemispheres, the extent of the open region is roughly 40° in longitude and 20° in latitude, though the shape and size change with viewing angle (Figures 7–12) and with the assumed magnetopause standoff distance (compare the compressed magnetopause mappings in Figures 14 and 15 to those for the expanded magnetopause).

[59] The flux equivalence calculation was performed only out to $R$ = 150 $R_J$, the limit of data availability and the valid region of the $B_N$ fit; however, the Jovian magnetotail is known to extend far beyond this distance. Estimates of the Jovian tail length range from ~900 $R_J$, based on Cassini data [*Krupp et al.*, 2004], to ~9000 $R_J$, based on Voyager 2 data [*Lepping et al.*, 1983]. More recently, New Horizons found that Jupiter's magnetotail possesses a coherent structure until at least ~1600 $R_J$ [*McNutt et al.*, 2007]; the spacecraft's trajectory took it into the magnetosheath beyond this distance. By assuming that field lines that cross the equator beyond 150 $R_J$ are open, we have undoubtedly overestimated the region of open flux in the ionosphere.

[60] We can correct for this overestimate and account for the magnetic flux that closes through the tail by assuming a radial dependence for $B_N$ and integrating the function from 150 to 9000 $R_J$. *Kivelson and Khurana* [2002] found that $B_z$, which on average is normal to the current sheet and can be considered equivalent to $B_N$, is given by

$$B_z(R) = 4.32 \times 10^4\, R^{-2.44}, \tag{7}$$

where $B_z$ is in nTs and $R$ is in Jovian radii. The magnetic flux closing through the equator in the magnetotail is therefore given by

$$\Phi_{equator} = \int_{R=150}^{R=9000} B_z(R)\, R\, d\phi\, dR = \int_{R=150}^{R=9000} 4.32 \times 10^4\, R^{-1.44}\, d\phi\, dR, \tag{8}$$

where we have carried out the integration to the greatest proposed tail length in order not to underestimate the amount of closed flux in the tail. Inclusion of the additional flux from 150 to 9000 $R_J$ shrinks the size of the polar cap by only approximately a few degrees of latitude, as we show by the red shaded region in Figure 17. The shape and boundaries of the red shaded region should not be taken literally; they are provided merely as illustrative examples such that the area of the red shaded region matches the ionospheric flux to the additional closed equatorial flux between 150 and 9000 $R_J$. We then identify the light and dark green shaded regions in Figure 17 as the polar cap. Its area is equivalent to that of a circle around the pole with an ~11° latitudinal width, only slightly smaller than the ~15° latitudinal width of the polar cap at the Earth.

[61] If the polar cap is accurately identified, the open flux linked to that region in the ionosphere should equal the tail lobe flux. We calculate that the open flux through the region we have identified as the polar cap in the northern ionosphere is $\sim 1.41 \times 10^5$ nT $R_J^2$ (~720 GWb); this number assumes that the area of open flux is associated with a compressed magnetopause and excludes the area that maps to radial distances from 150 to 9000 $R_J$ (Figure 17, red shaded region). We calculated the open flux by summing $B_R\, dA$ over the open region (Figure 17, light and dark green shaded regions), in bins of 1° of longitude by 1° of latitude. As discussed in section 4 above, the area of open flux is larger for the compressed magnetopause (Figure 17, green shaded regions) than for the expanded magnetopause (only the light green shaded region), so our estimate is on the high end of the range of expected values. A similar calculation for the southern hemisphere finds that the

**Figure 14.** Mapping results compared to auroral observations. (a) Mapping results for the expanded magnetopause locations of *Joy et al.* [2002]. The color of each contour indicates the radial distance, ranging from 20 $R_J$ (black) to 150 $R_J$ (red). The interior dashed black line indicates the location of the dark polar region in the study by *Stallard et al.* [2003]. (b) As for Figure 14a but for the compressed magnetosphere. (c) Contours for the expanded magnetopause color coded by the local time of the equatorial field line crossing. (d) UV auroral observations modified from Figure 5 in the study by *Grodent et al.* [2003b]. (e) A composite of the UV observations from Figure 14d and the mapping results of Figure 14a. The figures are presented with 160° SIII longitude directly to the bottom of the page and the direction of the Sun toward the bottom of the page and slightly to the left as indicated by arrows. The latitude and longitude grid separation is 10°. The boundaries of the three polar auroral regions are drawn in at the same jovicentric coordinates in all panels. The active region maps to just beyond the dayside magnetopause boundary, the swirl region maps to field lines outside of 150 $R_J$, and the dark region maps to both open and closed field lines. The main oval maps to ~15–30 $R_J$ near dawn, ~30–50 $R_J$ near noon, and 50–60 $R_J$ at ~1500 LT.

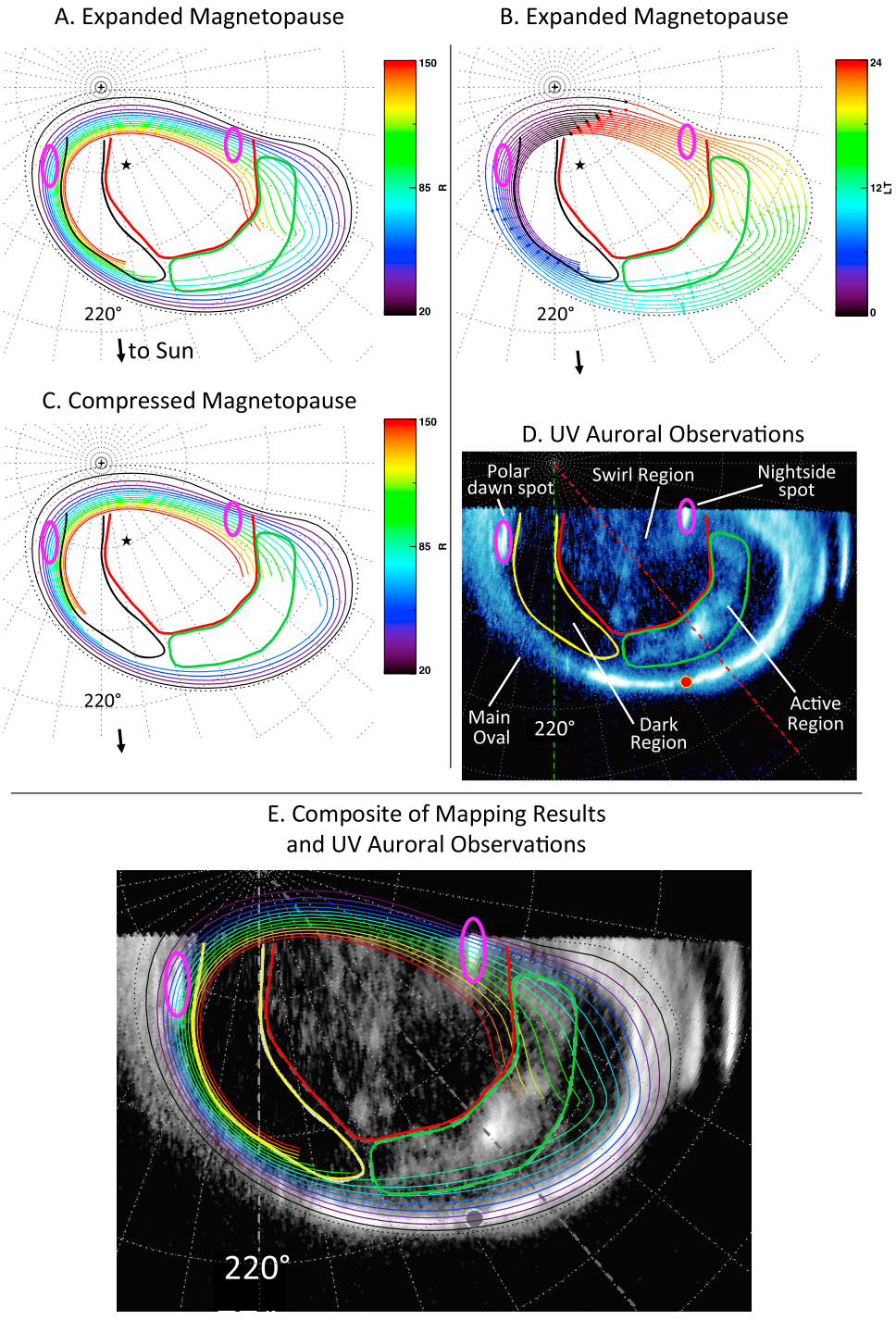


**Figure 15.** As in Figure 14 but for CML 202°. The active region continues to map just beyond the dayside magnetopause, and the swirl region maps to tail field lines outside of 150 $R_J$. The dark region now maps almost entirely to field lines beyond 150 $R_J$ in the predawn local time sector. The main oval maps to ~20–30 $R_J$ near dawn, ~30–50 $R_J$ prenoon, and 50–60 $R_J$ postnoon. Also shown are a polar dawn spot and a nightside spot, which map to distances inside of a statistical X line, consistent with the interpretation that these spots are the auroral signature of inward flow released during tail reconnection.

amount of open flux through the southern hemisphere is ~1.49 × $10^5$ nT $R_J^2$ (~762 GWb). The calculated values closely match the amount of open lobe flux in the magnetotail: magnetometer data show that $B_R$ ~ 7 nT at $R$ = 80 $R_J$, where the magnetotail width varies from 115 $R_J$ (compressed) to 165 $R_J$ (expanded) [*Joy et al.*, 2002]. Assuming a compressed magnetosphere with a width of 115 $R_J$, the lobe flux, $\int B \cdot dA$, is 7 nT × $\pi$ × (115 $R_J$)$^2$ × 1/2 = 1.45 × $10^5$ nT $R_J^2$

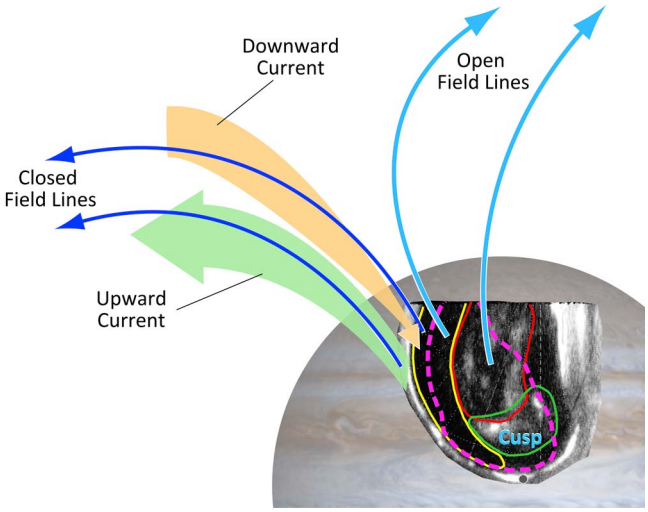


**Figure 16.** Schematic (not to scale) illustrating the mapping of Jupiter's polar auroral regions, which are outlined with colored contours as in Figure 14, to their magnetospheric sources. The open/closed flux boundary is shown as a dashed pink line. We interpret the active region as the Jovian polar cusp, the swirl region is interpreted as the open field lines of the polar cap, and the dark region maps to both open and closed field lines. Poleward of the open/closed flux boundary, open field lines (light blue) exit the ionosphere from both the dark and swirl regions and are pulled back toward the night side. A second field line, equatorward of the open/closed flux boundary, is shown emerging from the dark region. The light green arrow shows the upward (out of the ionosphere) field-aligned current associated with the main oval emissions, which are also on closed field lines. The orange arrow shows the closure or downward (into the ionosphere) field-aligned current, which could explain the relative lack of auroral emissions on closed field lines in the dark region.

(~741 GWb), very close to the amount of open flux through both the northern and southern ionosphere.

## 6. Discussion

[62] In section 4, we presented the flux equivalence calculation results, and in section 5, we compared the mapping to the auroral observations. We found that the polar auroral swirl region can be interpreted as the Jovian polar cap, and the polar auroral active region can be interpreted as linked to the Jovian polar cusp. In this section we address the previous assumption that most of the empty area interior to our contours maps to open flux. We also address the mapping of the cushion region. The section concludes with a brief comment on potential applications of our mapping results.

[63] What can we learn about global dynamics by mapping auroral features?

[64] Auroral observations can provide clues to the extent of the solar wind interaction with Jupiter's dayside magnetopause. For example, polar flares in the active region could be the signature of magnetic reconnection on a magnetopause Dungey cycle X line [*Grodent et al.*, 2003b] or the signature of a magnetospheric disturbance due to a sharp increase in the solar wind dynamic pressure [*Waite et al.*, 2001]. However, we have mapped the active region to an area beyond the dayside magnetopause, so it appears that only the most equatorward polar flares could map to the magnetopause.

[65] In our analysis, we interpreted empty areas (those mapping beyond the magnetopause or beyond 150 $R_J$ on the night side, roughly in the same location as the UV swirl region and the IR f-DPR) as being on open field lines. As quantified in section 5.2, this is an oversimplification because the magnetotail extends beyond 150 $R_J$; however, the amount of flux from 150 to 9000 $R_J$ is relatively small, so we feel justified in approximating the open/closed flux boundary by the 150 $R_J$ contour on the night side and by the magnetopause boundary on the day side. The empty areas may still not map to open field lines, however, if one assumes that Jupiter's magnetosphere is closed, following the arguments of *McComas and Bagenal* [2007]. They suggest that magnetic flux opened via dayside reconnection with the solar wind is closed on the magnetopause, near the polar cusps. As a result, Jupiter's polar cap would be expected to be small, only ~10° across, rather than the ~40° longitude by ~20° latitude we have suggested (Figure 17), and we feel that it is unlikely that the polar cap would be so small. *Cowley et al.* [2008] pointed out that it is difficult for cusp reconnection to close all of the flux opened on the day side. We do not find evidence to support the claim of *Delamere and Bagenal* [2010], who similarly proposed that Jupiter's magnetosphere is closed, that the f-DPR maps to the cushion region and region of viscous interaction between the solar wind and the magnetospheric flanks. Additionally, we have shown the flux through the empty area in both the northern and southern hemispheres very closely matches the

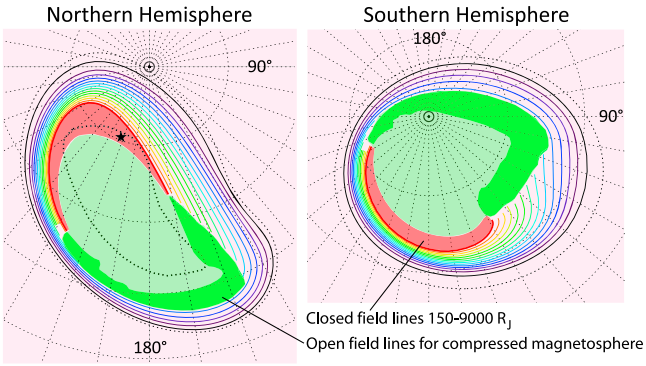


**Figure 17.** Summary of mapping results between the aurora and its magnetospheric sources for subsolar longitude 180°. The area mapping to closed field lines is shaded pink, and the region of closed flux accounted for by integrating $B_z$ from 150 to 9000 $R_J$ is shaded in red. The green shaded areas indicate the area mapping to beyond 150 $R_J$ or beyond the magnetopause, which we have interpreted as open flux. The dark green area maps to the region between the two preferred magnetopause locations (~60–90 $R_J$ at noon) and may be on open or closed field lines depending on which magnetopause location one assumes. Color scheme following *Bagenal* [2007, Figure 10].

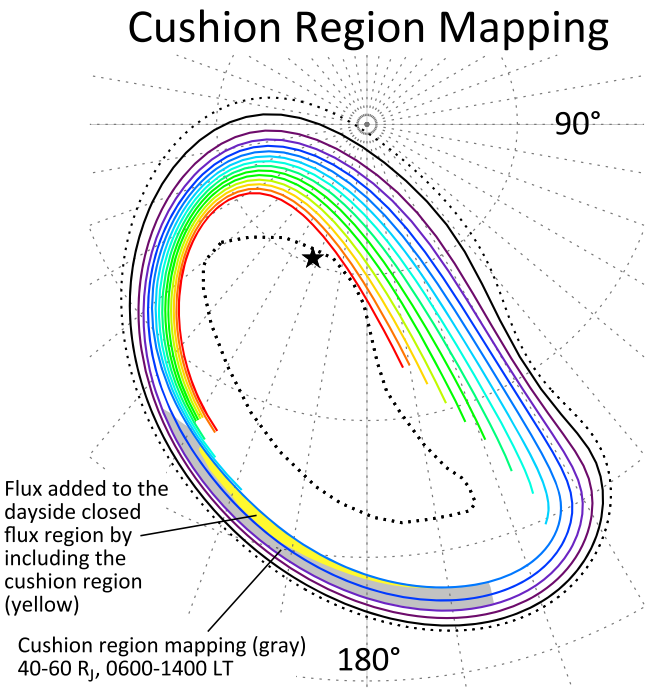


**Figure 18.** Cushion region mapping for subsolar longitude 180°, highlighted in gray. Assumed is a compressed magnetosphere, such that the cushion region is located at 40–60 $R_J$ and 0600–1400 LT. The yellow shaded region indicates the area of additional closed flux calculated by using a more realistic cushion region field value in the magnetosphere rather than an averaged value (see text).

open magnetic flux contained in the magnetotail lobes, further suggesting that this empty area in the ionosphere maps to open field lines. If we are correct, the question then becomes what processes produce the swirl region auroral emissions.

[66] The main oval emissions are associated with corotation enforcement currents and are not expected to map to a constant radial distance [*Grodent et al.*, 2003a]. Indeed, our analysis shows that the main oval mapping varies with local time. Near dawn, the main emissions map to ~20–30 $R_J$, while near dusk they map farther out, ~50–60 $R_J$. These results suggest that either the radial location of the corotation enforcement currents varies with local time, or the plasma outflow rate differs among local time sectors, or both. In a recent study of 9 years of HST data, *Grodent et al.* [2008a] found that the main oval location has shifted over time by as much as 3° in latitude. They proposed that the latitudinal shift could be explained by variations in the current sheet density or thickness and not just by a response to changing solar wind conditions. Similarly, we suggest that the main oval variation with local time seen here could be explained by a local time dependence on these current sheet properties or the plasma outflow rate.

[67] Thus far, we have concentrated on mapping auroral features to their magnetospheric sources, though it is also of interest to consider how certain magnetospheric features, such as the cushion region, map into the ionosphere. The cushion region is located in the postdawn to noon local time sector, at ~40–60 $R_J$ when the magnetopause is compressed and ~70–90 $R_J$ when the magnetopause is expanded. It has been suggested through theoretical arguments that the cushion region may be associated with the polar auroral dark region [*Kivelson and Southwood*, 2005]. However, our results show that the cushion region does not map to the auroral dark region but instead to the area just poleward of the main oval and just equatorward of the active region. Figure 18 shows a polar mapping for subsolar longitude with the cushion region mapping shaded in gray. For this mapping, we have assumed a compressed magnetosphere, such that the cushion region is located at a radial distance of 40–60 $R_J$, and have amended the $B_N$ model to more accurately match the measured cushion region field values. As previously discussed in section 4, the $B_N$ model represents a fit to data from all solar wind conditions, including magnetospheric expansions when the cushion region is located farther out, at 70–90 $R_J$. Therefore, we amended our $B_N$ model by approximating the field in the cushion region as 8 nT, typical of the larger field values in the 40–60 $R_J$ region (Figure 3). The yellow shaded region indicates the area of additional closed flux calculated by using this more realistic cushion region field value, with the assumption that the cushion region extends from 40 to 60 $R_J$ at local times 0600–1400. Figure 18 shows that the cushion region does not map to a large enough area to account for the polar dark region. We have accounted for possible underestimates in the field model and find that the correction does not significant affect our results.

[68] In order to facilitate use of our model, we have created a website that allows a user to magnetically map a point in Jupiter's ionosphere to the magnetosphere, and vice versa. This online mapping tool is available at the following link: http://www.igpp.ucla.edu/people/mvogt/mapping/.

[69] Although we defer further applications of our magnetic flux equivalence procedure, we note that the approach can be applied to additional matters of interest in Jovian dynamics. For example, it will be useful in establishing how the mapping of magnetospheric reconfiguration events [*Kronberg et al.*, 2005] and an associated X line [*Woch et al.*, 2002; *Vogt et al.*, 2010] compare to observed auroral polar dawn spots [*Radioti et al.*, 2008b]. Previous studies have mapped the polar dawn spots to their magnetospheric source regions (and vice versa) by tracing field lines from the available field models [*Radioti et al.*, 2008b; *Ge et al.*, 2010]. However, these models are not accurate beyond ~30 $R_J$, and both the tail reconnection events and the polar dawn spots occur on L shells beyond this distance. In section 5.1, we briefly discussed the mappings of two spots, a polar dawn spot and a nightside spot, seen in Figure 15. These spots both map to inside of the *Vogt et al.* [2010] statistical X line, consistent with the view that they are the signatures of inward flow associated with tail reconnection [*Radioti et al.*, 2010, 2011].

[70] Finally, we note that even with a novel approach such as the flux equivalence calculation we have performed here, we are still limited by the accuracy of the available internal field models. In our flux calculation, we assumed an initial ionospheric contour mapping to 15 $R_J$ based on the available internal field models. The field model used faithfully maps Ganymede's ionospheric footprint to an equatorial distance of 15 $R_J$, but as discussed in section 3.2, even at this dis-

tance the local time mapping is subject to an error of up to ~1.6 h. Therefore, another potential application of our mapping is to compare our results to a mapping obtained by simply following a field model from the equator to the ionosphere. Such a comparison would help us understand the limitations of the current Jovian field models and could facilitate the development of an improved model.

## 7. Summary

[71] This paper provides a reliable mapping between Jovian polar auroral features and their magnetospheric sources and establishes the size and location of Jupiter's polar cap and polar cusp. We have used a flux equivalence calculation based on the requirement that the magnetic flux through an area in the ionosphere equals the flux through the equatorial region to which it maps. This approach is preferred to tracing model field lines because the available magnetic field models are inaccurate at distances beyond ~30 $R_J$.

[72] Calculating the magnetic flux through the equator required a model for $B_N$, the component of the magnetic field normal to the current sheet. We developed a model, based on a fit to the available spacecraft data that accounts for changes with radial distance and local time. The local time dependence was of particular importance for accurately mapping local time asymmetries in the auroral emissions.

[73] We mapped equatorial field lines from 15 $R_J$, where auroral data have provided improved field models that can accurately reproduce the location of Ganymede's auroral footprint, out to 150 $R_J$ in the tail, the farthest limit of available spacecraft observations. However, this distance represents only a small fraction of the Jovian magnetotail, which is known to extend as far as ~9000 $R_J$. The additional equatorial flux between 150 and 9000 $R_J$ was found to shrink the size of the polar cap by only approximately a few degrees of latitude and does not greatly affect our conclusions relating to the need for an extended region of open flux in the polar cap.

[74] Our mapping reproduces several key auroral features. The region of open flux is shifted toward dawn because the equatorial $B_N$ (normal to the current sheet) is strongest in the afternoon local time sector. We find that the main oval mapping varies with local time, moving outward from ~15–30 $R_J$ near dawn to ~50–60 $R_J$ postnoon. The polar auroral active region maps to just outside the dayside magnetopause, a region that we identify as the Jovian polar cusp. The polar auroral swirl region maps to open tail field lines and is interpreted as the Jovian polar cap. These interpretations are consistent with some earlier predictions based on auroral observations (see section 2.3). The dark region mapping remains ambiguous, as it appears to be partly on open field lines and partly on closed field lines, and the mapping varies over a Jovian rotation period.

[75] Factors such as solar wind conditions are expected to affect the mapping results, but without an upstream solar wind monitor, it is difficult to determine quantitatively how changing solar wind conditions influence $B_N$ and modify the flux equivalence calculation. Therefore, in this paper, we presented a calculation using $B_N$ values averaged over all solar wind conditions, and our results are not fully representative of any particular solar wind condition. Despite the inconsistency of using averaged $B_N$ with specific magnetopause locations, we carried out magnetic flux mapping for two preferred magnetopause locations and for four different phases of a Jovian rotation period (similar to considering different viewing geometries or CMLs) to obtain contours that can be compared with auroral observations. Our contours change shape and orientation in ways that are distinctly similar to changes observed in the UV aurora, which gives us considerable confidence in the validity of the mapping we have done. We, therefore, believe that our conclusions regarding the source regions of auroral activity described by *Grodent et al.* [2003b] and by *Pallier and Prangé* [2001] are realistic.

[76] In addition to mapping the source of the polar auroral features, we argued that a significant fraction of the area inside the main oval emissions must map to open field lines. We have interpreted the empty area, or the area mapping beyond the magnetopause or beyond roughly 150 $R_J$ down the tail, as being on open field lines. Further justifying our interpretation is the fact that the flux through this empty area in both hemispheres very closely matches the open magnetic flux contained in the magnetotail lobes. We conclude that the size of Jupiter's polar cap is equivalent to a symmetric circle about the pole with an ~11° latitudinal width (though the Jovian polar cap itself is asymmetric). Alternate interpretations include the model of *McComas and Bagenal* [2007], who suggested that Jupiter's magnetosphere is closed and that the "empty" area in the ionosphere maps to closed field lines formed by a second reconnection with the solar wind at high latitudes (i.e., near the cusp), or of *Delamere and Bagenal* [2010], who also suggested that Jupiter's magnetosphere is closed but that the empty area maps instead to the cushion region and region of viscous interaction between the solar wind and the magnetospheric flanks. We feel that this is unlikely, particularly in view of the evidence that the flux through the empty area in the ionosphere is effectively the same as the flux through the lobes of the magnetotail.

[77] Finally, we have made our mapping results freely available online at http://www.igpp.ucla.edu/people/mvogt/mapping/. This Web site allows users to magnetically map a point in Jupiter's ionosphere to the magnetosphere, and vice versa.

[78] **Acknowledgments.** We thank Tom Stallard for helpful discussions regarding the infrared auroral observations and for kindly providing the coordinates of the fixed dark polar region. We also gratefully acknowledge helpful discussions with and constructive comments from Fran Bagenal. Finally, we thank Jack Connerney for consultation regarding the VIP4 model. PDS provided Voyager data. This work was supported in part by NASA grants NNX08AQ46G, NNX09AV91G, and NNG05GH41G. A.R. and D.G. were supported by the Belgian Fund for Scientific Research (FNRS) and the PRODEX program managed by the European Space Agency in collaboration with the Belgian Federal Science Policy Office.

[79] Masaki Fujimoto thanks Igor Alexeev and another reviewer for their assistance in evaluating this paper.

## References

Alexeev, I. I., and E. S. Belenkaya (2005), Modeling of the Jovian magnetosphere, *Ann. Geophys.*, *23*, 809–826, doi:10.5194/angeo-23-809-2005.

Bagenal, F. (2007), The magnetosphere of Jupiter: Coupling the equator to the poles, *J. Atmos. Sol. Terr. Phys.*, *69*, 387–402, doi:10.1016/j.jastp.2006.08.012.

Baron, R. L., T. Owen, J. E. P. Connerney, T. Satoh, and J. Harrington (1996), Solar wind control of Jupiter's $H_3^+$ auroras, *Icarus*, *120*, 437–442, doi:10.1006/icar.1996.0063.

Bonfond, B., D. Grodent, J.-C. Gérard, A. Radioti, V. Dols, P. Delamere, and J. Clarke (2009), The Io UV footprint: Location, inter-spot distances and tail vertical extent, *J. Geophys. Res.*, *114*, A07224, doi:10.1029/2009JA014312.

Clarke, J. T., et al. (1998), Hubble Space Telescope imaging of Jupiter's UV aurora during the Galileo orbiter mission, *J. Geophys. Res.*, *103*, 20,217–20,236, doi:10.1029/98JE01130.

Clarke, J. T., et al. (2002), Ultraviolet emissions from the magnetic footprints of Io, Ganymede and Europa on Jupiter, *Nature*, *415*, 997–1000, doi:10.1038/415997a.

Clarke, J. T., D. Grodent, S. W. H. Cowley, E. J. Bunce, P. Zarka, J. E. P. Connerney, and T. Satoh (2004), Jupiter's aurora, in *Jupiter: The Planet, Satellites, and Magnetosphere*, edited by F. Bagenal et al., pp. 639–670, Cambridge Univ. Press, New York.

Clarke, J. T., et al. (2009), Response of Jupiter's and Saturn's auroral activity to the solar wind, *J. Geophys. Res.*, *114*, A05210, doi:10.1029/2008JA013694.

Connerney, J., M. Acuña, and N. Ness (1981), Modeling the Jovian current sheet and inner magnetosphere, *J. Geophys. Res.*, *86*, 8370–8384, doi:10.1029/JA086iA10p08370.

Connerney, J. E. P., R. Baron, T. Satoh, and T. Owen (1993), Images of excited $H_3^+$ at the foot of the Io flux tube in Jupiter's atmosphere, *Science*, *262*, 1035–1038, doi:10.1126/science.262.5136.1035.

Connerney, J. E. P., M. H. Acuña, N. F. Ness, and T. Satoh (1998), New models of Jupiter's magnetic field constrained by the Io flux tube footprint, *J. Geophys. Res.*, *103*, 11,929–11,939, doi:10.1029/97JA03726.

Cowley, S. W. H., and E. J. Bunce (2001), Origin of the main auroral oval in Jupiter's coupled magnetosphere-ionosphere system, *Planet. Space Sci.*, *49*, 1067–1088, doi:10.1016/S0032-0633(00)00167-7.

Cowley, S. W. H., E. J. Bunce, T. S. Stallard, and S. Miller (2003), Jupiter's polar ionospheric flows: Theoretical interpretation, *Geophys. Res. Lett.*, *30*(5), 1220, doi:10.1029/2002GL016030.

Cowley, S. W. H., S. V. Badman, S. M. Imber, and S. E. Milan (2008), Comment on "Jupiter: A fundamentally different magnetospheric interaction with the solar wind" by D. J. McComas and F. Bagenal, *Geophys. Res. Lett.*, *35*, L10101, doi:10.1029/2007GL032645.

Delamere, P. A., and F. Bagenal (2010), Solar wind interaction with Jupiter's magnetosphere, *J. Geophys. Res.*, *115*, A10201, doi:10.1029/2010JA015347.

Ge, Y. S., C. T. Russell, and K. K. Khurana (2010), Reconnection sites in Jupiter's magnetotail and relation to Jovian auroras, *Planet. Space Sci.*, *58*, 1455–1469, doi:10.1016/J.PSS.2010.06.013.

Grodent, D., J. T. Clarke, J. Kim, J. H. Waite, and S. W. H. Cowley (2003a), Jupiter's main auroral oval observed with HST-STIS, *J. Geophys. Res.*, *108*(A11), 1389, doi:10.1029/2003JA009921.

Grodent, D., J. T. Clarke, J. H. Waite Jr., S. W. H. Cowley, J.-C. Gérard, and J. Kim (2003b), Jupiter's polar auroral emissions, *J. Geophys. Res.*, *108*(A10), 1366, doi:10.1029/2003JA010017.

Grodent, D., J.-C. Gérard, J. T. Clarke, G. R. Gladstone, and J. H. Waite (2004), A possible auroral signature of a magnetotail reconnection process on Jupiter, *J. Geophys. Res.*, *109*, A05201, doi:10.1029/2003JA010341.

Grodent, D., J.-C. Gérard, A. Radioti, B. Bonfond, and A. Saglam (2008a), Jupiter's changing auroral location, *J. Geophys. Res.*, *113*, A01206, doi:10.1029/2007JA012601.

Grodent, D., B. Bonfond, J.-C. Gérard, A. Radioti, J. Gustin, J. T. Clarke, J. Nichols, and J. E. P. Connerney (2008b), Auroral evidence of a localized magnetic anomaly in Jupiter's northern hemisphere, *J. Geophys. Res.*, *113*, A09201, doi:10.1029/2008JA013185.

Gurnett, D. A., W. S. Kurth, and F. L. Scarf (1980), The structure of the Jovian magnetotail from plasma wave observations, *Geophys. Res. Lett.*, *7*(1), 53–56, doi:10.1029/GL007i001p00053.

Gurnett, D. A., et al. (2002), Control of Jupiter's radio emission and aurorae by the solar wind, *Nature*, *415*, 985–987, doi:10.1038/415985a.

Hanlon, P. G., M. K. Dougherty, N. Krupp, K. C. Hansen, F. J. Crary, D. T. Young, and G. Tóth (2004), Dual spacecraft observations of a compression event within the Jovian magnetosphere: Signatures of externally triggered supercorotation? *J. Geophys. Res.*, *109*, A09S09, doi:10.1029/2003JA010116.

Hill, T. W. (1979), Inertial limit on corotation, *J. Geophys. Res.*, *84*, 6554–6558, doi:10.1029/JA084iA11p06554.

Hill, T. W. (2001), The Jovian auroral oval, *J. Geophys. Res.*, *106*, 8101–8107, doi:10.1029/2000JA000302.

Joy, S. P., M. G. Kivelson, R. J. Walker, K. K. Khurana, C. T. Russell, and T. Ogino (2002), Probabilistic models of the Jovian magnetopause and bow shock locations, *J. Geophys. Res.*, *107*(A10), 1309, doi:10.1029/2001JA009146.

Khurana, K. K. (1997), Euler potential models of Jupiter's magnetospheric field, *J. Geophys. Res.*, *102*, 11,295–11,306, doi:10.1029/97JA00563.

Khurana, K. K. (2001), Influence of solar wind of Jupiter's magnetosphere deduced from currents in the equatorial plane, *J. Geophys. Res.*, *106*, 25,999–26,016, doi:10.1029/2000JA000352.

Khurana, K. K., and M. G. Kivelson (1993), Inference of the angular velocity of plasma in the Jovian magnetosphere from the sweepback of magnetic field, *J. Geophys. Res.*, *98*, 67–79, doi:10.1029/92JA01890.

Khurana, K. K., and H. K. Schwarzl (2005), Global structure of Jupiter's magnetospheric current sheet, *J. Geophys. Res.*, *110*, A07227, doi:10.1029/2004JA010757.

Kivelson, M. G., and K. K. Khurana (2002), Properties of the magnetic field in the Jovian magnetotail, *J. Geophys. Res.*, *107*(A8), 1196, doi:10.1029/2001JA000249.

Kivelson, M. G., and D. J. Southwood (2005), Dynamical consequences of two modes of centrifugal instability in Jupiter's outer magnetosphere, *J. Geophys. Res.*, *110*, A12209, doi:10.1029/2005JA011176.

Kronberg, E. A., J. Woch, N. Krupp, A. Lagg, K. K. Khurana, and K.-H. Glassmeier (2005), Mass release at Jupiter: Substorm-like processes in the Jovian magnetotail, *J. Geophys. Res.*, *110*, A03211, doi:10.1029/2004JA010777.

Kronberg, E. A., K.-H. Glassmeier, J. Woch, N. Krupp, A. Lagg, and M. K. Dougherty (2007), A possible intrinsic mechanism for the quasi-periodic dynamics of the Jovian magnetosphere, *J. Geophys. Res.*, *112*, A05203, doi:10.1029/2006JA011994.

Krupp, N., J. Woch, A. Lagg, S. Livi, D. G. Mitchell, S. M. Krimigis, M. K. Dougherty, P. G. Hanlon, T. P. Armstrong, and S. A. Espinosa (2004), Energetic particle observations in the vicinity of Jupiter: Cassini MIMI/LEMMS results, *J. Geophys. Res.*, *109*, A09S10, doi:10.1029/2003JA010111.

Lepping, R. P., M. D. Desch, L. W. Klein, E. C. Sittler Jr., J. D. Sullivan, W. S. Kurth, and K. W. Behannon (1983), Structure and other properties of Jupiter's distant magnetotail, *J. Geophys. Res.*, *88*, 8801–8815, doi:10.1029/JA088iA11p08801.

Marklund, G. T. (2009), Electric fields and plasma processes in the auroral downward current region, below, within, and above the acceleration region, *Space Sci. Rev.*, *142*, 1–21, doi:10.1007/s11214-008-9373-9.

McComas, D. J., and F. Bagenal (2007), Jupiter: A fundamentally different magnetospheric interaction with the solar wind, *Geophys. Res. Lett.*, *34*, L20106, doi:10.1029/2007GL031078.

McNutt, R. L., Jr., et al. (2007), Energetic particles in the Jovian magnetotail, *Science*, *318*, 220–222, doi:10.1126/science.1148025.

Nichols, J. D., E. J. Bunce, J. T. Clarke, S. W. H. Cowley, J.-C. Gérard, D. Grodent, and W. R. Pryor (2007), Response of Jupiter's UV auroras to interplanetary conditions as observed by the Hubble Space Telescope during the Cassini flyby campaign, *J. Geophys. Res.*, *112*, A02203, doi:10.1029/2006JA012005.

Ogino, T., R. Walker, and M. Kivelson (1998), A global magnetohydrodynamic simulation of the Jovian magnetosphere, *J. Geophys. Res.*, *103*, 225–235, doi:10.1029/97JA02247.

Pallier, L., and R. Prangé (2001), More about the structure of the high latitude Jovian aurorae, *Planet. Space Sci.*, *49*, 1159–1173, doi:10.1016/S0032-0633(01)00023-X.

Prangé, R., G. Chagnon, M. G. Kivelson, T. A. Livengood, and W. Kurth (2001), Temporal monitoring of Jupiter's auroral activity with IUE during the Galileo mission. Implications for magnetospheric processes, *Planet. Space Sci.*, *49*, 405–415, doi:10.1016/S0032-0633(00)00161-6.

Radioti, A., J.-C. Gérard, D. Grodent, B. Bonfond, N. Krupp, and J. Woch (2008a), Discontinuity in Jupiter's main auroral oval, *J. Geophys. Res.*, *113*, A01215, doi:10.1029/2007JA012610.

Radioti, A., D. Grodent, J.-C. Gérard, B. Bonfond, and J. T. Clarke (2008b), Auroral polar dawn spots: Signatures of internally driven reconnection processes at Jupiter's magnetotail, *Geophys. Res. Lett.*, *35*, L03104, doi:10.1029/2007GL032460.

Radioti, A., A. T. Tomás, D. Grodent, J.-C. Gérard, J. Gustin, B. Bonfond, N. Krupp, J. Woch, and J. D. Menietti (2009), Equatorward diffuse auroral emissions at Jupiter: Simultaneous HST and Galileo observations, *Geophys. Res. Lett.*, *36*, L07101, doi:10.1029/2009GL037857.

Radioti, A., D. Grodent, J.-C. Gérard, and B. Bonfond (2010), Auroral signatures of flow bursts released during magnetotail reconnection at Jupiter, *J. Geophys. Res.*, *115*, A07214, doi:10.1029/2009JA014844.

Radioti, A., D. Grodent, J.-C. Gérard, M. F. Vogt, M. Lystrup, and B. Bonfond (2011), Nightside reconnection at Jupiter: Auroral and magnetic field observations from July 26, 1998, *J. Geophys. Res.*, doi:10.1029/2010JA016200, in press.

Satoh, T., and J. E. P. Connerney (1999), Jupiter's $H_3^+$ emissions viewed in corrected jovimagnetic coordinates, *Icarus*, *141*, 236–252, doi:10.1006/icar.1999.6173.

Southwood, D. J., and M. G. Kivelson (2001), A new perspective concerning the influence of the solar wind on the Jovian magnetosphere, *J. Geophys. Res.*, *106*, 6123–6130, doi:10.1029/2000JA000236.

Stallard, T. S., S. Miller, S. W. H. Cowley, and E. J. Bunce (2003), Jupiter's polar ionospheric flows: Measured intensity and velocity variations poleward of the main auroral oval, *Geophys. Res. Lett.*, *30*(5), 1221, doi:10.1029/2002GL016031.

Vasavada, A. R., A. H. Bouchez, A. P. Ingersoll, B. Little, and C. D. Anger (1999), Jupiter's visible aurora and Io footprint, *J. Geophys. Res.*, *104*, 27,133–27,142, doi:10.1029/1999JE001055.

Vasyliūnas, V. M. (1983), Plasma distribution and flow, in *Physics of the Jovian Magnetosphere*, edited by A. J. Dessler, 395 pp., Cambridge Univ. Press, New York.

Vogt, M. F., M. G. Kivelson, K. K. Khurana, S. P. Joy, and R. J. Walker (2010), Reconnection and flows in the Jovian magnetotail as inferred from magnetometer observations, *J. Geophys. Res.*, *115*, A06219, doi:10.1029/2009JA015098.

Waite, J. H., Jr., et al. (2001), An auroral flare at Jupiter, *Nature*, *410*, 787–789, doi:10.1038/35071018.

Woch, J., N. Krupp, A. Lagg, B. Wilken, S. Livi, and D. J. Williams (1998), Quasi-periodic modulations of the Jovian magnetotail, *Geophys. Res. Lett.*, *25*, 1253–1256, doi:10.1029/98GL00861.

Woch, J., N. Krupp, and A. Lagg (2002), Particle bursts in the Jovian magnetosphere: Evidence for a near-Jupiter neutral line, *Geophys. Res. Lett.*, *29*(7), 1138, doi:10.1029/2001GL014080.

Zieger, B., and K. C. Hansen (2008), Statistical validation of a solar wind propagation model from 1 to 10 AU, *J. Geophys. Res.*, *113*, A08107, doi:10.1029/2008JA013046.

B. Bonfond, K. K. Khurana, M. G. Kivelson, M. F. Vogt, and R. J. Walker, Institute of Geophysics and Planetary Physics, UCLA, Box 951567, 6844D Slichter Hall, Los Angeles, CA 90095, USA. (marissav@ucla.edu)

D. Grodent and A. Radioti, LPAP, Institut d'Astrophysique et de Géophysique, Université de Liège, B-4000 Liège, Belgium.